A synthesis of thermokarst lake water balance in high-latitude regions of North America from isotope tracers

Lauren A. MacDonald, Brent B. Wolfe, Kevin W. Turner, Lesleigh Anderson, Christopher D. Arp, S. Jean Birks, Frédéric Bouchard, Thomas W.D. Edwards, Nicole Farquharson, Roland I. Hall, Ian McDonald, Biljana Narancic, Chantal Ouimet, Reinhard Pienitz, Jana Tondu, and Hilary White

June 2017

NRC Research Press

ARTICLE

A synthesis of thermokarst lake water balance in high-latitude regions of North America from isotope tracers[1]

Lauren A. MacDonald, Brent B. Wolfe, Kevin W. Turner, Lesleigh Anderson, Christopher D. Arp, S. Jean Birks, Frédéric Bouchard, Thomas W.D. Edwards, Nicole Farquharson, Roland I. Hall, Ian McDonald, Biljana Narancic, Chantal Ouimet, Reinhard Pienitz, Jana Tondu, and Hilary White

Abstract: Numerous studies utilizing remote sensing imagery and other methods have documented that thermokarst lakes are undergoing varied hydrological transitions in response to recent climate changes, from surface area expansion to drainage and evaporative desiccation. Here, we provide a synthesis of hydrological conditions for 376 lakes of mainly thermokarst origin across high-latitude North America. We assemble surface water isotope compositions measured during the past decade at five lake-rich landscapes including Arctic Coastal Plain (Alaska), Yukon Flats (Alaska), Old Crow Flats (Yukon), northwestern Hudson Bay Lowlands (Manitoba), and Nunavik (Quebec). These landscapes represent the broad range of thermokarst environments by spanning gradients in meteorological, permafrost, and vegetation conditions. An isotope framework was established based on flux-weighted long-term averages of meteorological conditions for each lake to quantify water balance metrics. The isotope composition of source water and evaporation-to-inflow ratio for each lake were determined, and the results demonstrated a substantial array of regional and subregional diversity of lake hydrological conditions. Controls on lake water balance and how these vary among the five landscapes and with differing environmental drivers are assessed. Findings reveal that lakes in the Hudson Bay Lowlands are most vulnerable to evaporative desiccation, whereas those in Nunavik are most resilient. However, we also identify the complexity in predicting hydrological responses of these thermokarst landscapes to future climate change.

Key words: thermokarst lakes, high-latitude regions, water isotope tracers, hydrology, permafrost, climate change.

Received 14 June 2016. Accepted 3 November 2016.

L.A. MacDonald, B.B. Wolfe, N. Farquharson, and H. White. Department of Geography and Environmental Studies, Wilfrid Laurier University, 75 University Avenue West, Waterloo, ON N2L 3C5, Canada.
K.W. Turner. Department of Geography, Brock University, St. Catharines, ON L2S 3A1, Canada.
L. Anderson. Geosciences and Environmental Change Science Center, US Geological Survey, Denver, CO 80225, USA.
C.D. Arp. Water and Environmental Research Centre, University of Alaska Fairbanks, Fairbanks, AK 99775, USA.
S.J. Birks. InnoTech Alberta, Calgary, AB T2L 2A6, Canada; Department of Geography, University of Victoria, Victoria, BC V8W 3R4, Canada.
F. Bouchard, B. Narancic, and R. Pienitz. Département de Géographie, Université Laval, QC G1V 0A6, Canada.
T.W.D. Edwards. Department of Earth and Environmental Sciences, University of Waterloo, Waterloo, ON N2L 3G1, Canada.
R.I. Hall and J. Tondu. Department of Biology, University of Waterloo, Waterloo, ON N2L 3G1, Canada.
I. McDonald. Yukon Field Unit, Parks Canada, Whitehorse, YT Y1A 2B5, Canada.
C. Ouimet. Parks Canada Agency, Churchill, MB R0B 0E0, Canada.
Corresponding author: Lauren A. MacDonald (email: L7macdon@uwaterloo.ca).
[1]This article is part of a Special issue entitled "Arctic permafrost systems".
Brent B. Wolfe currently serves as an Associate Editor; peer review and editorial decisions regarding this manuscript were handled by Warwick Vincent.

Résumé : De nombreuses études utilisant des images de télédétection et d'autres méthodes ont porté à notre connaissance que les lacs thermokarstiques subissent des transitions hydrologiques diverses en réponse aux changements climatiques récents, soit de l'expansion de leur superficie au drainage et à la dessiccation par l'évaporation. Ici, nous fournissons une synthèse des conditions hydrologiques de 376 lacs d'origine principalement thermokarstique, et ce, à travers les hautes latitudes en Amérique du Nord. Nous assemblons des compositions isotopiques d'eau de surface mesurées au cours de la dernière décennie et provenant de cinq régions abondantes en lacs y compris la plaine côtière de l'Arctique (Alaska), la plaine du Yukon (Alaska), la plaine Old Crow (Yukon), les basses terres de la baie d'Hudson du nord-ouest (Manitoba) et le Nunavik (Québec). Ces régions représentent la vaste gamme d'environnements thermokarstiques couvrant des gradients de conditions météorologiques, de pergélisol et de végétation. Un cadre d'isotopes a été établi en fonction des moyennes à long terme pondérées par le flux des conditions météorologiques pour chaque lac afin de quantifier les paramètres du bilan hydraulique. On a déterminé la composition des isotopes d'eau de source et le rapport entre l'évaporation et le débit entrant pour chaque lac et les résultats ont indiqué que les conditions hydrologiques des lacs s'étalent sur une gamme substantielle de diversité régionale et sous régionale. On évalue les contrôles en matière du bilan hydraulique des lacs et comment ceux-ci varient entre les cinq régions et selon les différents facteurs environnementaux. Les résultats révèlent que les lacs des basses terres de la baie d'Hudson sont les plus vulnérables à la dessiccation par évaporation, tandis que ceux dans le Nunavik sont les plus résistants. Cependant, nous définissons aussi la complexité quant à la prédiction des réponses hydrologiques de ces régions thermokarstiques à la suite de changement climatique futur.

Mots-clés : lacs thermokarstiques, régions de hautes latitudes, traceur d'isotope d'eau, hydrologie, pergélisol, changement climatique.

Introduction

Thermokarst lakes and ponds (hereafter referred to collectively as lakes) are plentiful across permafrost terrain, occupying 15%–50% of the landscape in northwestern Canada, Siberia, and Alaska (e.g., Mackay 1988; Rampton 1988; Frohn et al. 2005; Grosse et al. 2005; Plug et al. 2008). Thermokarst lakes form as ice-rich permafrost thaws and surface water accumulates where subsidence occurs. These shallow waterbodies (generally <10 m deep and frequently <2 m) are a key component of northern hydrological and biogeochemical cycles, provide habitat and resources for wildlife and waterfowl populations, and support the traditional lifestyle of many indigenous communities. During the past few decades, increasing air temperatures and changes in precipitation patterns have been observed throughout much of the Arctic (e.g., ACIA 2004; IPCC 2013). Understanding the effects of climate change on thermokarst lake water balance is particularly important, as the greatest effects on aquatic ecosystems will occur indirectly via alteration of hydrological processes and their cascading influences on limnology, biogeochemistry, and aquatic ecology rather than from simply air temperature rise (Rouse et al. 1997; Prowse et al. 2006; Schindler and Smol 2006; Tranvik et al. 2009). Indeed, numerous studies have sought to document the hydrological status of thermokarst lakes. Many of these studies indicate that thermokarst lake hydrology is changing rapidly (e.g., Smith et al. 2005; Carroll et al. 2011), but along varying trajectories including surface area expansion, rapid drainage, and evaporative desiccation (e.g., Yoshikawa and Hinzman 2003; Riordan et al. 2006; Labrecque et al. 2009; Rowland et al. 2010; Bouchard et al. 2013).

Understanding the myriad of potential responses of thermokarst lake hydrology to ongoing climate change requires knowledge of their water balances ($\Delta S/\Delta T$, i.e., change in storage (S) over time (T)), which can be generally characterized as follows (Turner et al. 2010):

$$\Delta S/\Delta T = P_S + P_R + I_{OW} + I_S - E - O_{GW} - O_S \quad (1)$$

Positive contributors to thermokarst lake water balance include snowmelt (P_S), rainfall (P_R), subsurface inflow (I_{GW}), and surface channelized inflow (I_S), whereas lake water loss may occur via evaporation (E), subsurface outflow (O_{GW}), and surface outflow (O_S) — the latter potentially occurring catastrophically. Relative roles of hydrological processes that control thermokarst lake water balances may be influenced by a variety of drivers, including meteorological and permafrost (continuous, discontinuous, and sporadic) conditions as primary drivers (e.g., Riordan et al. 2006; Plug et al. 2008; Labrecque et al. 2009). Changes in temperature can alter rates of evaporation (E), while changes in precipitation regimes can lead to direct fluctuations in snowmelt (P_S) and rainfall (P_R) input, surface channelized inflow (I_S), and surface outflow (O_S). Consequently, high rates of evaporation with low snowmelt or rainfall supply can cause lakes to desiccate, while low rates of evaporation and abundant supply from precipitation may result in attaining maximum basin capacity, which can lead to shoreline erosion and lake expansion or even rapid lateral lake drainage (e.g., Riordan et al. 2006; Hinkel et al. 2007; Plug et al. 2008; Marsh et al. 2009; Turner et al. 2010; Jones et al. 2011; MacDonald et al. 2012; Bouchard et al. 2013). A warming climate also causes increased permafrost degradation, which can influence thermokarst lake hydrological status (e.g., Yoshikawa and Hinzman 2003; Smith et al. 2005). For many thermokarst lakes, continuous permafrost impedes subsurface inflow (I_{GW}) and outflow (O_{GW}) from contributing significantly to lake water balance. However, as permafrost degrades, subsurface flow pathways can develop, which can lead to vertical lake drainage (e.g., Yoshikawa and Hinzman 2003; Jepsen et al. 2013). Additionally, landscape characteristics, such as catchment vegetation, strongly influence thermokarst lake water balance (Bouchard et al. 2013; Turner et al. 2014). For example, densely forested areas entrap snow, which results in enhanced snowmelt runoff to lakes during spring (P_S) compared to runoff generated in more sparsely vegetated areas.

Deciphering the relative influence of hydrological processes represented in eq. 1 is challenging, especially for lake-rich permafrost landscapes where there may be substantial spatial heterogeneity among lakes and their catchments. Due to logistical constraints of field work in remote locations, it is often impractical to perform direct conventional measurements of hydrological processes on a spatially extensive set of lakes that is required to capture the potential diversity of prevailing conditions. Alternatively, and especially for multiple lake studies across landscapes, measurement of water isotope composition (δ^2H and $\delta^{18}O$) and application of isotope mass-balance models can be used to provide information of hydrological interest, as has recently been demonstrated for the continental United States (Brooks et al. 2014). For remote locations in particular, analysis of lake water isotope compositions is an excellent alternative to more instrument-intensive hydrological approaches. Surface water samples can easily and quickly be obtained during fieldwork, and their isotope compositions are sensitive to hydrological processes that influence lake water balances because systematic and well-understood isotopic fractionation of water occurs as it passes through the hydrological cycle (Edwards et al. 2004; Darling et al. 2006). Thus, the isotope composition of water provides quantitative information on lake water balance conditions, including the relative contributions of input waters (e.g., snowmelt, rain, and permafrost thaw waters as "δ_I values") and the relative importance of evaporation (frequently expressed as an evaporation-to-inflow ratio (E/I)). Water isotope analysis has been applied in several northern and remote landscapes on thermokarst as well as other shallow lake systems, yielding novel insight into the diversity and importance of hydrological processes on lake water balances spanning multiple environmental gradients

(e.g., Gibson and Edwards 2002; Brock et al. 2007; Yi et al. 2008; Turner et al. 2010, 2014; Anderson et al. 2013; Tondu et al. 2013; Arp et al. 2015).

As an outcome of the Natural Sciences and Engineering Research Council of Canada Discovery Frontiers ADAPT (Arctic Development and Adaptation to Permafrost in Transition) project (Vincent et al. 2013), we provide a synthesis and snapshot of water balance conditions for 376 lakes in high-latitude North America that mainly formed by thermokarst processes. Specifically, we assemble surface water isotope compositions measured during summers of the past decade from mainly thermokarst lakes across five expansive lake-rich permafrost landscapes. From west to east, these include Arctic Coastal Plain (Alaska) (Arp et al. 2015), Yukon Flats (Alaska) (Anderson et al. 2013), Old Crow Flats (Yukon) (Turner et al. 2010, 2014; Tondu et al. 2013), western Hudson Bay Lowlands (Manitoba) (Bouchard et al. 2013), and Nunavik (Quebec) (Narancic et al. 2017). We use isotope–mass balance modeling to determine lake input–water isotope compositions and E/I ratios and explore their relations among landscapes and with environmental drivers. Results provide a unique opportunity to rank hydrological vulnerability of these lake-rich permafrost landscapes and to predict hydrological responses to various climate change scenarios. While most of these data have been previously published as part of individual landscape hydrological studies, to our knowledge, the present analysis is the first, broad spatial synthesis of lake water balance status across lake-rich permafrost landscapes of North America.

Methods

Study areas

The five study regions (Fig. 1) selected for this synthesis collectively span broad gradients in permafrost, catchment vegetation, and meteorological conditions and contain abundant thermokarst lakes that have been previously sampled and analyzed for water isotope composition. The Arctic Coastal Plain (ACP) north of the Brooks Range in Alaska including lands between Barrow and Prudhoe Bay contains abundant shallow lakes mainly of thermokarst origin, is underlain by continuous permafrost, and contains tundra vegetation (Arp and Jones 2009). The Yukon Flats (YF) spans ~118 000 km^2 and is set along the Yukon River floodplain and its terraces south of the Brooks Range in Alaska. This lowland interior landscape is located within the zone of discontinuous permafrost and contains over 40 000 lakes of thermokarst, fluvial, and eolian origin (Williams 1962; Arp and Jones 2009). Catchment vegetation includes grassy meadows and muskeg to spruce and birch forests (Anderson et al. 2013). Old Crow Flats (OCF) spans 5600 km^2 and is situated ~55 km north of the village of Old Crow in northern Yukon Territory. This low-relief landscape is located within an area of continuous permafrost and contains over 2700 shallow primarily thermokarst lakes (Lauriol et al. 2002; Turner et al. 2014). Vegetation in OCF is variable and captures a gradient from spruce forest to tall shrubs to tundra vegetation (Turner et al. 2014). The western Hudson Bay Lowlands (HBL) spans 475 000 km^2 and contains over 10 000 shallow mainly thermokarst lakes. The HBL is underlain by discontinuous permafrost in the southwest and continuous permafrost in the northeast. Vegetation ranges from boreal spruce forest in the southwest to arctic tundra in the northeast (Rouse 1991; Duguay and Lafleur 2003). Nunavik (NUN), located north of the 55° parallel along the eastern coast of Hudson Bay in northern Quebec, contains abundant thermokarst lakes. Permafrost ranges from sporadic in the south to discontinuous in the north (Allard and Séguin 1987; Brown et al. 2002). Vegetation is mainly spruce–lichen forest in the south and shrub tundra in the north.

Lakes included in this study are considered mainly thermokarst in origin. However, they include a small number of lakes of fluvial and eolian origin in YF, oxbow lakes in OCF, and

Fig. 1. Location of study regions and their relations with permafrost category. Permafrost spatial data are from Brown et al. (2002).

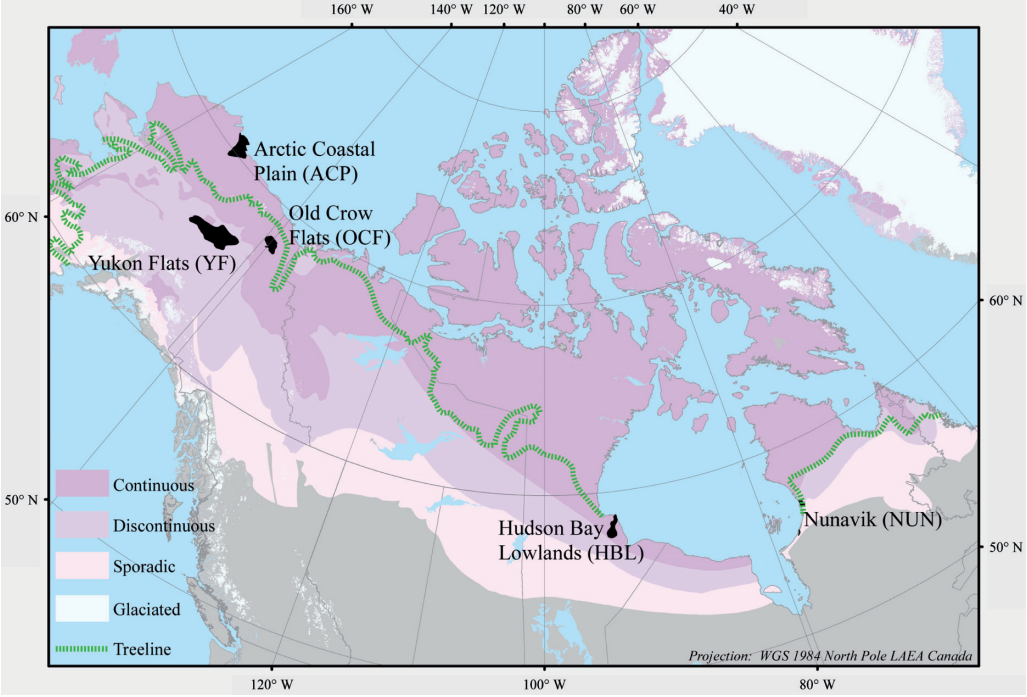

lakes located in topographic depressions between former beach ridges in HBL. These are included in this synthesis because they constitute a portion of the shallow aquatic ecosystems in these landscapes and for simplicity, we refer to "thermokarst lakes" as all encompassing. Thermokarst lakes from which isotope data have been obtained tend to be shallow and range in surface area (ACP: 0.6–16.2 m, 0.04–9.8 km^2; YF: 1–30 m, 0.017–5 km^2 (Anderson et al. 2013); OCF: 0.47–4.15 m, 2×10^{-3} – 13.181 km^2 (Turner et al. 2010); HBL: ~ < 0.5 m, < 7×10^{-4} – 7.6 km^2 (Bouchard et al. 2013); NUN: 1–5 m, ~1.3×10^{-6} to 2.1×10^{-3} km^2 (Bouchard et al. 2014; Narancic et al. 2017)).

A common gridded climate database was used to compile regional meteorological records for comparative purposes, to provide necessary parameters for water isotope mass balance modeling, and to gain insight of meteorological influence on lake water balances. The New et al. (2002) gridded climate database was selected due to the availability of lake-specific meteorological data and the ease of use of the database for a large data set, even though it predates our sampling intervals. Mean annual, summer, and winter temperatures and precipitation vary substantially among the five landscapes, based on mean monthly values for 1961–1990 (Fig. 2). Mean annual temperature ranges from −10.5 °C (ACP) to −5.3 °C (NUN) and annual precipitation ranges from 141 mm (ACP) to 580 mm (NUN) (Fig. 2*a*). ACP and OCF have lower mean annual temperature and precipitation than the other landscapes. YF has relatively low mean annual precipitation but high mean annual temperature, while HBL and NUN have relatively high mean annual temperature and precipitation. Similar patterns exist for mean winter temperature and winter precipitation, with mean winter temperature ranging from −19.2 °C (OCF) to −16.2 °C (NUN) and winter precipitation ranging from 53 mm (ACP) to 182 mm (NUN) (Fig. 2*b*). Mean summer temperature ranges from 5.6 °C (NUN) to 9.8 °C (YF) and summer precipitation ranges from 88 mm (ACP) to 399 mm (NUN) (Fig. 2*c*). Compared to mean annual and winter meteorological data, similar patterns

Fig. 2. Average landscape values for (a) mean annual temperature and mean annual precipitation, (b) mean winter temperature and mean winter precipitation, and (c) mean summer temperature and mean summer precipitation extracted from the New et al. (2002) climate database. Winter and summer intervals were defined by mean monthly temperatures below and above 0 °C, respectively.

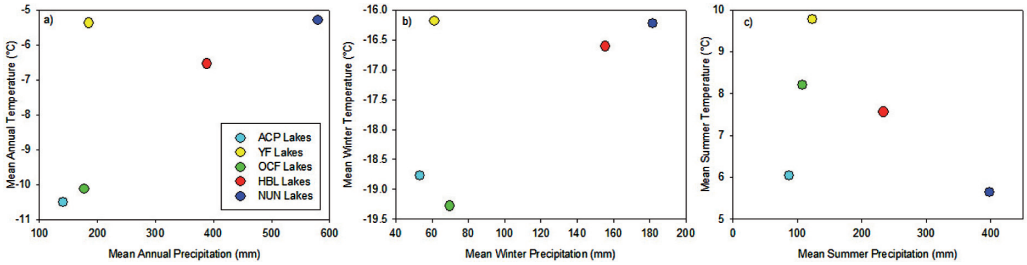

for ACP, YF, and OCF are evident for summer temperature and summer precipitation. However, HBL has a more midrange mean summer temperature and NUN has the lowest mean summer temperature.

Isotope hydrology

We assembled water isotope compositions (δ^2H and $\delta^{18}O$) for 376 lakes sampled during the past decade in the five study regions. Forty-four lakes were sampled during August 2015 in ACP, 149 lakes were sampled once during the summer between 2007 and 2011 in YF (Anderson et al. 2013), 53 lakes were sampled each summer from 2007 to 2009 and four additional lakes were sampled in 2007 and 2009 in OCF (Turner et al. 2010, 2014), 40 lakes were sampled in the summer of 2010 in HBL and 37 lakes were sampled in the summers of 2011–2012 (Bouchard et al. 2013), and 86 lakes were sampled from one to four times during summers 2011–2014 in NUN (Narancic et al. 2017). Samples were collected at 10–15 cm water depth in either 30 mL high density polyethylene bottles or 20 mL scintillation vials with plastic cone-shaped caps. Samples were transported back to the field base and then shipped to the Alaska Stable Isotope Facility at the University of Alaska Fairbanks (ACP), University of Arizona Environmental Isotope Laboratory (YF), or the University of Waterloo Environmental Isotope Laboratory (OCF, HBL, and NUN) for determination of hydrogen and oxygen isotope compositions using standard mass spectrometric techniques (Epstein and Mayeda 1953; Morrison et al. 2001), with the exception of NUN samples collected in 2014, which were analyzed using Off-Axis Integrated Cavity Output Spectroscopy. Isotope composition results are reported in δ notation, which represents deviations in per mil from Vienna Standard Mean Ocean Water (VSMOW) and are normalized to −428‰ and −55.5‰ for δ^2H and $\delta^{18}O$, respectively, for Standard Light Antarctic Precipitation (Coplen 1996). We restricted our analysis to July and August sample collection time periods to reduce seasonal effects caused by the influence of snowmelt while also capturing the expected midsummer peak in evaporation. For lakes that were sampled more than once per summer (July and August), or over multiple summers, we used the average value in our analyses.

Isotope framework development

Raw water isotope compositions were initially assessed in conventional $\delta^{18}O$–δ^2H space, superimposed upon an "isotope framework" consisting of the Global Meteoric Water Line (GMWL) and the Local Evaporation Line (LEL) predicted for each landscape (Fig. 3). The GMWL, described by $\delta^2H = 8\delta^{18}O + 10$ (Craig 1961), reflects the isotopic distribution of global precipitation. The position of amount-weighted precipitation along the GMWL is mainly dependent on the distillation history of atmospheric moisture contributing to precipitation

Fig. 3. Schematic $\delta^{18}O$–$\delta^{2}H$ diagram illustrating an approach for the interpretation of lake water isotope data within a region. Key features include the Global Meteoric Water Line (GMWL), the landscape-predicted Local Evaporation Line (LEL), average annual isotope composition of precipitation (δ_P), the terminal basin steady-state isotope composition (δ_{SSL}), the limiting non-steady-state isotope composition (δ^*), lake water isotope composition (δ_L), input water isotope composition (δ_I), and the isotope composition of evaporated vapour from the lake (δ_E).

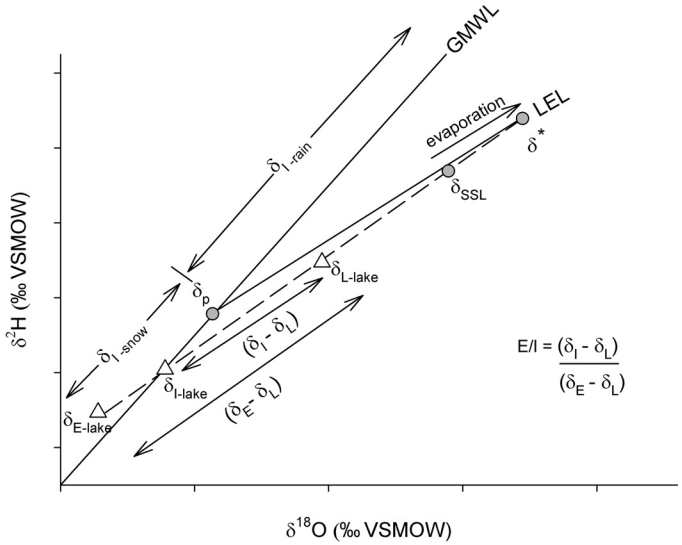

and commonly leads to snow plotting along an isotopically depleted portion of the GMWL relative to rain (Fig. 3). Surface water isotope compositions, including lakes, typically plot along a LEL, which generally has a slope of 4–6 (Fig. 3). The LEL for a given landscape, as applied in this context, defines the expected isotopic evolution of a surface waterbody undergoing evaporation, fed by waters representing the average annual isotope composition of precipitation (δ_P) for that region. Displacement of water compositions along the LEL from δ_P reflects evaporative loss, while deviation from the LEL is often indicative of mixing with source waters such as snowmelt or rainfall, which tend to plot along the GMWL (Fig. 3). Key reference points along the LEL include the terminal (i.e., closed-drainage) basin steady-state isotope composition (δ_{SSL}), which represents the special case of a waterbody at hydrologic and isotopic steady-state in which evaporation exactly equals inflow and the limiting non-steady-state isotope composition (δ^*), which indicates the maximum potential transient isotopic enrichment of a waterbody as it approaches complete desiccation (Fig. 3).

For each landscape, the LEL was predicted using the linear resistance model of Craig and Gordon (1965) following similar approaches presented in Brock et al. (2007) and Wolfe et al. (2011). Hereafter, we refer to this as the "landscape-predicted LEL." Predicting the LEL, rather than the more commonly used empirical technique of applying linear regression through measured lake water isotope compositions, allows lake water isotope compositions to be interpreted independently based on their position along (degree of evaporation) and about (i.e., above/below; relative influence of different input waters such as snowmelt and rainfall) the LEL (e.g., see Tondu et al. 2013; Turner et al. 2014).

The following equations were used to develop the landscape-predicted LELs and are expressed in decimal notation. The equilibrium liquid–vapour fractionation factors (α^*)

for oxygen and hydrogen are dependent on temperature and have been determined empirically by Horita and Wesolowski (1994), where

$$(2)\quad 1000 \ln \alpha^* = -7.685 + 6.7123(10^3/T) - 1.6664(10^6/T^2) + 0.35041(10^9/T^3)$$

for $\delta^{18}O$ and

$$(3)\quad 1000 \ln \alpha^* = 1158.8(T^3/10^9) - 1620.1(T^2/10^6) + 794.84(T/10^3) - 161.04 + 2.9992(10^9/10^3)$$

for δ^2H, where T represents the interface temperature in K. ε^* is the temperature-dependent equilibrium separation between liquid and vapour water given by

$$(4)\quad \varepsilon^* = \alpha^* - 1$$

and kinetic separation (ε_K) is expressed by

$$(5)\quad \varepsilon_K = C_K(1 - h)$$

where constant enrichment values (C_K) for oxygen and hydrogen are 0.0142 and 0.0125, respectively, and h is relative humidity (Gonfiantini 1986). δ_{AS} is the isotope composition of ambient open-water season atmospheric moisture, often assumed to be in isotopic equilibrium with evaporation-flux-weighted local open-water season precipitation (δ_{PS}) (Gibson et al. 2008) such that

$$(6)\quad \delta_{AS} = (\delta_{PS} - \varepsilon^*)/\alpha^*$$

The limiting isotopic enrichment of a waterbody approaching desiccation (δ^*) has been defined by Gonfiantini (1986) and can be determined from

$$(7)\quad \delta^* = (h\delta_{AS} + \varepsilon_K + \varepsilon^*/\alpha^*)/(h - \varepsilon_K - \varepsilon^*/\alpha^*)$$

δ_{SSL} represents the isotope composition of a terminal basin in which evaporation is exactly compensated by inflow, as defined by Gonfiantini (1986)

$$(8)\quad \delta_{SSL} = \alpha^*\delta_I(1 - h - \varepsilon_K) + \alpha^* h\delta_{AS} + \alpha^*\varepsilon_K + \varepsilon^*$$

where the isotope composition of inflow, δ_I, is assumed to be equal to δ_P. The landscape-predicted LEL was determined by linear regression through δ_P and δ^*.

Water-balance metrics

The water balance metrics, δ_I and E/I ratios, were determined for each of the 376 lakes using the Yi et al. (2008) coupled-isotope tracer approach, which assumes conservation of mass and isotope composition during evaporation. According to mass conservation, the isotope composition of evaporated vapour from a lake (δ_E) will lie on the extension of the lake-specific LEL to the left of the GMWL (Fig. 3) and was determined from the formulation provided by Gonfiantini (1986), where δ_L is the measured lake water isotope composition:

$$(9)\quad \delta_E = ((\delta_L - \varepsilon^*)/\alpha^* - h\delta_{AS} - \varepsilon_K)/(1 - h - \varepsilon_K)$$

Values for δ_I were derived from calculating lake-specific evaporation lines and their intersection with the GMWL, which reasonably assumes that input waters are nonevaporated and plot on the GMWL and that all lake-specific evaporation lines converge at δ^* (Yi et al. 2008) (Fig. 3). The relative contributions of rainfall and snowmelt were then assessed by evaluating the position of δ_I compared to the landscape value of δ_P along the GMWL. For example, δ_I values that were more isotopically enriched than δ_P were categorized as *rainfall-dominated* lakes and δ_I values that were more isotopically depleted than δ_P were categorized as *snowmelt-dominated* lakes. For some YF lakes, very low δ_I values are interpreted as lakes fed primarily by permafrost thaw waters (see below and Anderson et al. 2013).

E/*I* ratios, which provide a snapshot of water balance through the mass-balance relation of evaporation to inflow, were calculated from Gibson and Edwards (2002):

$$(10) \quad E/I = (\delta_I - \delta_L)/(\delta_E - \delta_L)$$

An *E*/*I* ratio of 0.5 represents lakes where 50% of the inflow has evaporated, and we use this threshold to define *evaporation-dominated* lakes (after Tondu et al. 2013). As applied here, *E*/*I* ratios estimate net evaporative loss in midsummer and can indicate whether lake water volumes are increasing ($E/I << 1$) or decreasing ($E/I > 1$) where no drainage outlet exists. This approach assumes a well-mixed lake at isotopic steady-state; thus, values greater than 1 are inconsistent with the assumptions in the model but are used comparatively to identify lakes strongly influenced by evaporation.

Model input climate parameters, *T* and *h*, for calculation of the landscape-predicted LELs and lake water balance metrics were derived from the New et al. (2002) gridded climate database, which provided output for individual lake coordinates. This approach was used in the isotope mass-balance modeling of the individual lakes to account for spatial gradients in meteorological conditions within and among landscapes. Monthly *T* and *h* averages for the open-water season were flux-weighted according to potential evaporation using Thornthwaite (1948) for each landscape and for each of the 376 lakes. Values for δ_P (to anchor the landscape-predicted LEL) and δ_{PS} (used to determine δ_{As}; eq. 6 for both the landscape-predicted LEL and each individual lake to account for spatial variations) were extracted from "The online isotopes in precipitation calculator" (waterisotopes.org; Bowen 2016). This database uses global precipitation oxygen and hydrogen isotope data to calculate average monthly and annual δ_P values for any given location and elevation (Bowen et al. 2005). Sampling year(s) meteorological conditions (temperature, relative humidity, and precipitation) for a representative location from each landscape were extracted from the NCEP North American Regional Reanalysis (NARR 2015) monthly composites and compared with the 1961–1990 landscape averages from the New et al. (2002) gridded database to assess the representativeness of meteorological conditions during the specific sampling years.

The influence of catchment vegetation on the water-balance metrics was assessed after land cover for each lake was broadly classified as *tundra dominant* or *forest dominant*. Tundra-dominant vegetation included catchments with high proportions of dwarf shrubs and areas of sparse vegetation, while forest-dominant vegetation included lake catchments with high proportions of deciduous and coniferous woodland or forest and tall shrub vegetation. Vegetation classes for ACP and YF were determined using the USGS National Land Cover Database of Alaska. For OCF, vegetation classes were simplified based on analysis of a Landsat 5 TM mosaic (Turner et al. 2014). Vegetation type for HBL and NUN was identified based on visual observations during field work.

Nonparametric Kruskal–Wallis statistical tests were conducted to assess whether *E*/*I* distributions differed among lakes in different permafrost zones (continuous, discontinuous, and sporadic) and between vegetation categories (forest dominant versus tundra dominant) and whether $\delta^{18}O_I$ values differed among lakes in the different vegetation categories. When Kruskal–Wallis tests involving the permafrost zones produced a significant result ($P \leq 0.05$), pairwise comparisons were conducted using Dunnett's post hoc tests. All statistical tests were performed using the software SPSS version 20. *E*/*I* values for lakes that were evaporating under strongly non-steady-state conditions ($E/I > 1$) were set to 1.5 for boxplot analyses and the statistical tests.

Results

Meteorological conditions during sampling years

Comparison of specific sampling year meteorological conditions (NARR) with the 1961–1990 average values (New et al. 2002) for each landscape reveals some similarities

Fig. 4. Comparison of average sampling year (solid bars, NARR 2015) and 1961–1990 average (grey bars, New et al. 2002) values for summer temperature, summer relative humidity, summer precipitation, and winter precipitation for the five landscapes.

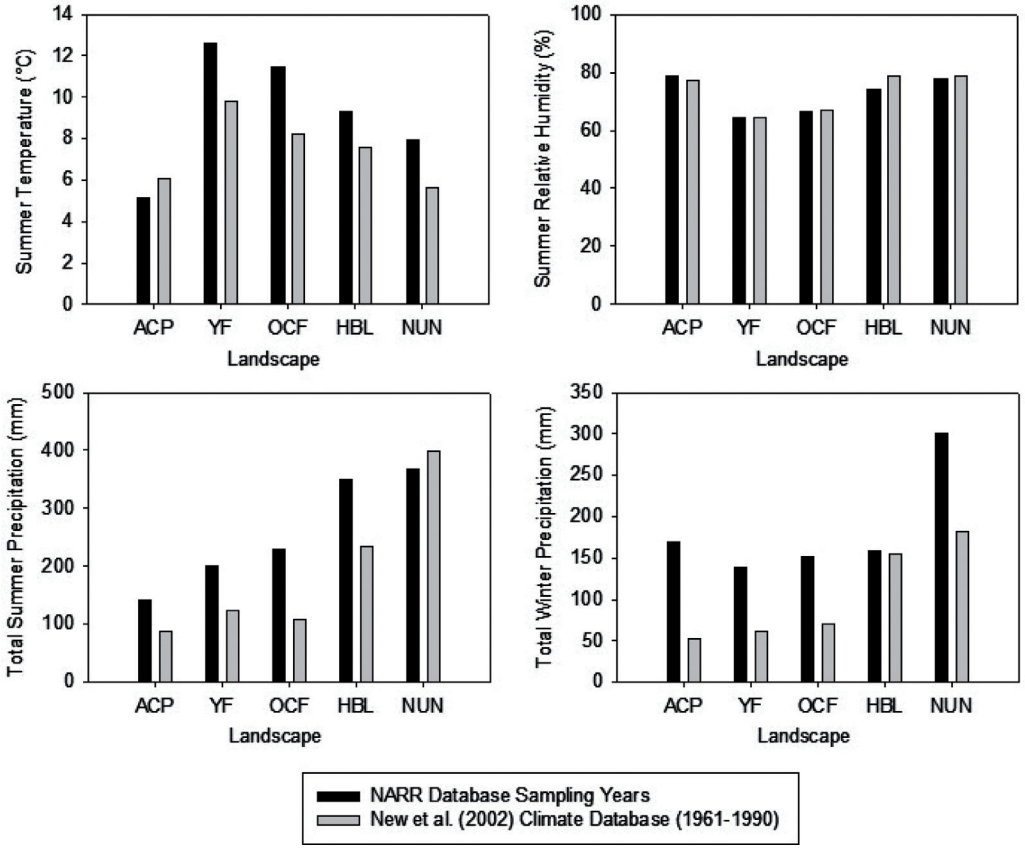

and differences (Fig. 4). Summer temperatures were higher (1.8–3.3 °C) during sampling years for YF, OCF, HBL, and NUN landscapes than the 1961–1990 average. At ACP, the summer temperatures were lower (0.9 °C) than the 1961–1990 average. Humidity values for the sampling years were similar to the 1961–1990 averages at all five landscapes. Precipitation shows the greatest difference between the values for the sampling years versus the 1961–1990 average. During the sampling years, ACP, YF, and OCF had consistently higher summer (54–121 mm) and winter precipitation (78–115 mm) than the 1961–1990 average, while HBL had higher summer precipitation (115 mm) during sampling years when compared to the 1961–1990 averages. In contrast, NUN had lower summer precipitation (32 mm) and higher winter precipitation (119 mm) during sampling years when compared to the 1961–1990 averages.

Isotope hydrology

Lake water isotope compositions (δ_L)

Lake water isotope compositions (δ_L) from all of the assembled data range from −20.5‰ to −2.4‰ and from −168.7‰ to −53.0‰ for $\delta^{18}O$ and $\delta^{2}H$, respectively (Appendix; Fig. 5). The wide range of δ_L values reflects the diverse lake hydrological conditions at the time of sampling in these high-latitude regions. YF has the greatest range of δ_L values, indicating substantial within-landscape variability, while NUN has the smallest range, signifying that lakes possess a narrower range of hydrological conditions in this landscape.

Fig. 5. Water isotope compositions (δ_L) from 376 lakes superimposed onto the landscape-specific isotope frameworks. The data defining the landscape-predicted LELs are shown in Table 1.

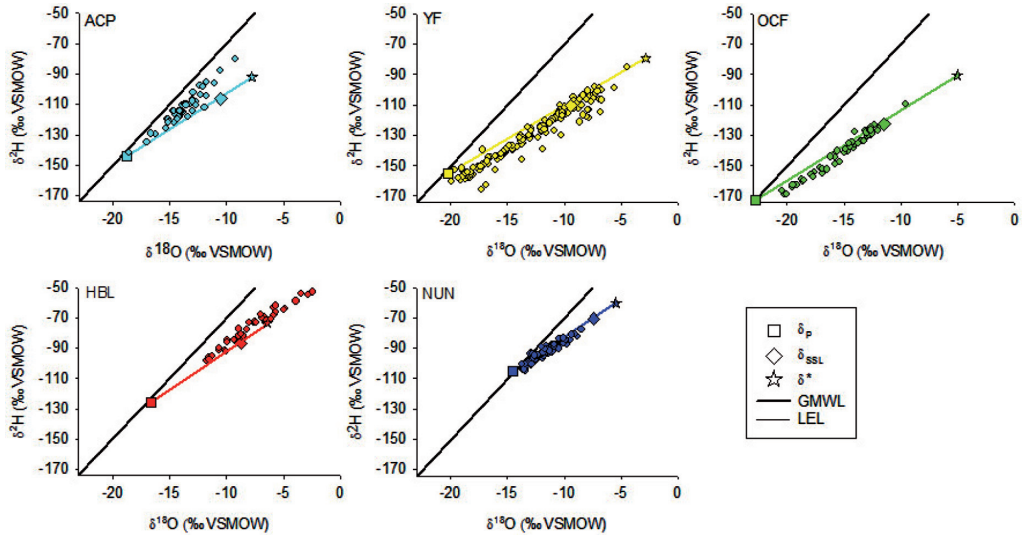

For each of the five landscapes, δ_L values form a linear trend that typically plot along a similar trajectory as the landscape-predicted LELs, supporting the contention that the frameworks are reasonable approximations of isotopic evaporative trajectories (Fig. 5). Indeed, the landscape-predicted LELs are in close agreement with the empirically defined LELs, except for ACP (Table 1). For ACP, δ_L values plot along a trajectory with a somewhat steeper slope than the landscape-predicted LEL, likely due to high rainfall immediately prior to sampling (Fig. 4). The LELs and δ_L values for OCF and YF, and HBL and NUN, are positioned in similar $\delta^{18}O$–$\delta^{2}H$ space, likely reflecting similar latitudes and the associated well-known effect on isotope composition of precipitation (Rozanski et al. 1993). ACP, the most northerly landscape, does not follow this pattern, perhaps due to its closer proximity to the Arctic coast and associated reduced continental influence on precipitation isotope composition. δ_L values from NUN are evenly distributed about the LEL, while δ_L values from HBL and ACP typically plot above their respective LELs, suggesting a stronger influence of rainfall compared to snowmelt on lake water balance. Conversely, δ_L values from YF and OCF generally plot below their respective LELs, reflecting a stronger influence of snowmelt compared to rainfall on water balances. Additionally, a small group of lakes (n = 15) from YF have δ_L values that plot on a particularly low trajectory (i.e., parallel to, but offset below, the landscape-predicted LEL), which Anderson et al. (2013) suggested reflect more dominant input by isotopically depleted water from permafrost thaw in this region (elaborated on in the next section). δ_L values from HBL are positioned farthest away from the GMWL on the LEL, with many lakes plotting beyond δ_{SSL} and some approaching and surpassing the landscape-predicted δ^*, indicating strong non-steady-state evaporative isotopic enrichment at the time of sampling. In contrast, δ_L values from NUN are positioned closest to the GMWL on the LEL, indicating that lakes in this landscape are least influenced by evaporation.

Source water identification (δ_I)

The isotope composition of lake-specific input water (δ_I) was calculated for each lake in the five landscapes to evaluate the relative roles of different source waters on lake hydrological conditions (Fig. 6). Lake-specific $\delta^{18}O_I$ values range from −38.6‰ to −7.2‰ and lake-specific $\delta^{2}H_I$ values range from −298.4‰ to −47.7‰. The large range in δ_I values illustrates

Table 1. Parameters used to construct the landscape-specific isotopic frameworks.

Parameter	ACP	YF	OCF	HBL	NUN	Equation(s)	Source
h (%)	76	63	65	78	79		New et al. (2002)
T (K)	280.7	284.2	283.3	283.7	281.2		New et al. (2002)
α^* (^{18}O, ^{2}H)	1.0110, 1.1005	1.0106, 1.0955	1.0107, 1.0968	1.0107, 1.0962	1.0109, 1.0997	2, 3	Horita and Wesolowski (1994)
ε^* (^{18}O, ^{2}H) (‰)	11.0, 100.5	10.6, 95.5	10.7, 96.8	10.7, 96.2	10.9, 99.7	4	Gonfiantini (1986)
ε_k (^{18}O, ^{2}H) (‰)	3.5, 3.1	5.3, 4.6	5.0, 4.4	3.1, 2.8	3.0, 2.6	5	Gonfiantini (1986)
δ_{As} (^{18}O, ^{2}H) (‰)	−26.6, −205	−27.8, −213	−29.1, −221	−23.9, 181	−22.9, −171	6	Gibson and Edwards (2002)
δ^* (^{18}O, ^{2}H) (‰)	−7.8, −92	−2.8, −79	−5.0, −90	−6.4, −74	−5.4, −60	7	Craig and Gordon (1965)
δ_{SSL} (^{18}O, ^{2}H) (‰)	−10.5, −106	−9.4, −110	−11.5, −123	−8.7, −87	−7.4, −71	8	Gibson and Edwards (2002)
δ_P (^{18}O, ^{2}H) (‰)	−18.8, −144	−20.2, −155	−22.7, −173	−16.6, −126	−14.5, −105		Bowen 2016)
δ_{Ps} (^{18}O, ^{2}H) (‰)	−15.9, −126	−17.5, −138	−18.7, −146	−13.5, −103	−12.2, −89		Bowen (2016)
L-P LEL	$4.67*\delta^{18}O$-55.9	$4.37*\delta^{18}O$-66.8	$4.63*\delta^{18}O$-67.2	$5.10*\delta^{18}O$-41.0	$4.98*\delta^{18}O$-33.0		
L-E LEL	$6.40*\delta^{18}O$-24.9	$4.64*\delta^{18}O$-70.1	$5.41*\delta^{18}O$-59.4	$4.91*\delta^{18}O$-38.3	$4.28*\delta^{18}O$-42.6		

Note: h, humidity; T, temperature; α^*, equilibrium liquid–vapour fractionation factor; ε^*, temperature-dependent equilibrium separation between liquid and vapour water; ε_K, kinetic separation; $\delta_{AS,}$ isotope composition of ambient open-water season atmospheric moisture; δ^*, limiting non-steady-state isotope composition; δ_{SSL}, terminal basin steady-state isotope composition; δ_P, average annual isotope composition of precipitation; δ_{PS}, average open-water season isotope composition of precipitation; L-P LEL, landscape-predicted Local Evaporation Line; L-E LEL, empirically defined Landscape Local Evaporation Line. ACP, Arctic Coastal Plain; Alaska; YF, Yukon Flats; OCF, Old Crow Flats; HBL, Hudson Bay Lowlands; NUN, Nunavik.

Fig. 6. Isotope compositions of lake-specific input water (δ_I) for each of the five landscapes. Classification of snowmelt-dominated lakes ($\delta_I \leq \delta_P$), rainfall-dominated lakes ($\delta_I > \delta_P$), and permafrost thaw-dominated lakes ($\delta_I << \delta_P$) are represented by the diagonal lines. Note the different axis scales.

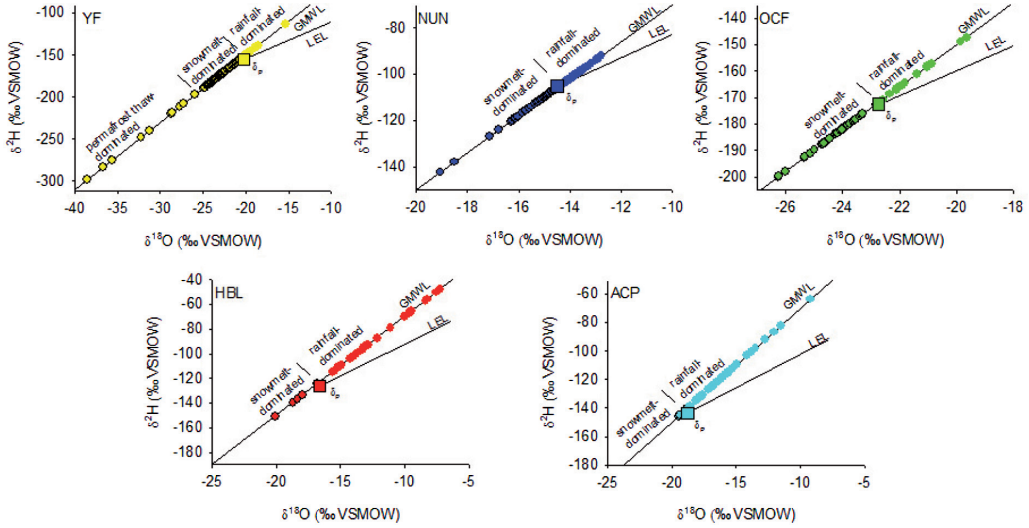

the high variability in the average proportion of source water type (i.e., rain and snowmelt) to all lakes within and among the landscapes. YF lakes possess the largest range of δ_I values, indicating substantial within-landscape variability in the proportions of source water types, while lakes in NUN have the smallest range of δ_I values, signifying less variability in proportions of source water type. Lakes with the lowest δ_I values are found in YF, while lakes in HBL have the highest δ_I values.

For each landscape, δ_I values were compared with the mean annual isotope composition of precipitation value (δ_P) to classify lakes as snowmelt ($\delta_I \leq \delta_P$) versus rainfall ($\delta_I > \delta_P$) dominated (Fig. 6). YF and OCF have the highest proportions of snowmelt-dominated lakes, 89% and 72%, respectively, indicating the strong influence of snowmelt on lake water balances in these landscapes, even during midsummer sampling. Of note, there was a small group of lakes in YF with particularly low δ_I values, likely due to input from snowmelt and permafrost thaw (Anderson et al. 2013). YF is underlain by discontinuous permafrost, and the observed values were within the range of values for permafrost thaw waters in this area (Meyer et al. 2010; Lachniet et al. 2012; Anderson et al. 2013). Slightly more than half of the lakes (52%) in NUN are snowmelt dominated, indicating a more even distribution of snowmelt versus rainfall source waters throughout the landscape. Some rainfall-dominated lakes in NUN may also be fed by permafrost thaw waters (Narancic et al. 2017). Rainfall-dominated lakes are the overwhelming majority in HBL (80%) and ACP (91%), reflecting the strong influence of rainfall on lake water balances in these landscapes at the time of sampling.

Evaporation-to-inflow (E/I) estimates

Evaporation-to-inflow ratios (*E*/*I*) were calculated for each lake in the five different landscapes to evaluate the relative importance of vapour loss on lake hydrological conditions (Fig. 7). The 376 lakes span a wide spectrum of *E*/*I* values, from close to 0 to much greater than 1, illustrating a range of water balances from those dominated by input waters to those dominated by evaporation. Overall, 219 lakes (58%) have $E/I < 0.5$, while 157 lakes (42%) have $E/I > 0.5$ (i.e., >50% evaporative water loss), which we consider as evaporation dominated. Calculated *E*/*I* distributions vary among landscapes (Fig. 7). For NUN and ACP, the vast

Fig. 7. Cumulative proportions (lines, right *y*-axis) and frequency (bars, left *y*-axis) distributions of *E*/*I* values for thermokarst lakes from the five landscapes. The vertical broken line represents *E*/*I* = 0.5. Water balance of lakes with *E*/*I* > 0.5 is considered evaporation dominated. Note the varying vertical scales.

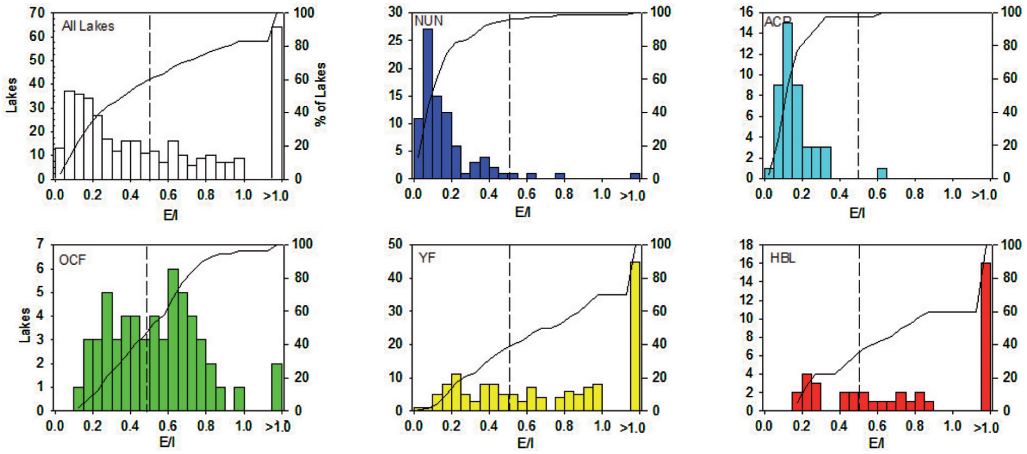

majority of lakes (95% and 98%, respectively) have *E*/*I* < 0.5. Lakes in OCF have a relatively even distribution with *E*/*I* < 0.5 in 46% of lakes. In contrast, a majority of lakes in YF and HBL have *E*/*I* > 0.5 (63% and 68%, respectively), and these two regions have the largest proportion of lakes with *E*/*I* > 1 (30% and 40%, respectively). In HBL and YF, *E*/*I* > 1 is consistent with field observations of lakes throughout the landscape having undergone desiccation by midsummer (Anderson et al. 2013; Bouchard et al. 2013).

Discussion

Thermokarst lakes have been undergoing hydrological transitions in response to recent climate change (e.g., Yoshikawa and Hinzman 2003; Smith et al. 2005; Riordan et al. 2006; Labrecque et al. 2009; Rowland et al. 2010; Carroll et al. 2011; Bouchard et al. 2013). Our analysis of water isotope compositions and calculations of δ_I and *E*/*I* ratios for 376 lakes at five lake-rich permafrost landscapes (ACP, YF, OCF, HBL, and NUN) in arctic and subarctic North America indicate that the importance of input types (rainfall, snowmelt, and permafrost) and evaporation are highly variable. Results show that striking similarities and differences in thermokarst lake hydrology exist among landscapes. Large gradients in δ_I occur within and among landscapes and identify that lakes in HBL and ACP are mainly rainfall dominated, whereas lakes in OCF and YF are mainly snowfall dominated. Lakes in NUN have roughly equal proportions of rainfall- and snowfall-dominated lakes. Snowfall-dominated lakes from YF also likely include lakes with substantial contributions from permafrost thaw water (and possibly also in NUN, although these are isotopically indistinguishable from rainfall-dominated lakes; Narancic et al. 2017). *E*/*I* values span from almost 0 to much greater than 1. Most lakes in ACP and NUN have *E*/*I* < 0.5, while the majority of lakes in YF and HBL are evaporation dominated despite higher-than-normal (1961–1990) precipitation during sampling years. These findings underscore the strong hydrological gradients that exist across thermokarst lakes from high-latitude regions. In the discussion below, we first acknowledge assumptions and uncertainties in the isotope modeling approach. Then, relations of δ_I and *E*/*I* ratios with climate and catchment characteristics among the five landscapes are explored, which provide the basis for anticipating how thermokarst lake hydrology in these northern regions may change in the future.

Assumptions and uncertainties

The nature of this broad continental-scale meta-analysis necessarily assumes that lakes sampled are representative of their landscapes and required decisions to ensure a consistent modeling approach given availability of existing data. Water balance metrics derived in this study were calculated from a single lake water isotope measurement or an average of July and August lake water isotope measurements over multiple years and thus they represent a snapshot of conditions. Also, the specific sampling years varied among the five landscapes. Although comparing water isotope data from different years for the five landscapes may result in some inherent variability, it is unlikely that the interannual variability for a single lake would exert a strong influence on comparisons within and among the five landscapes given the large range of lake water isotope compositions and E/I and δ_I values across the landscapes. We explored this for landscapes where multiple years of summer water isotope measurements were available (OCF, HBL, and NUN), and indeed, spatial variability far exceeded annual summer variability of individual lakes. For OCF, the range in $\delta^{18}O$ and $\delta^{2}H$ values for all lakes was 11.9‰ (minimum = −21.0‰, maximum = −9.1‰) and 64.6‰ (minimum = −172.3‰, maximum = −107.7‰), respectively. In contrast with the large spatial variability, the greatest range for an individual lake in OCF over the 3 year sampling period was 2.3‰ and 11.9‰ for $\delta^{18}O$ and $\delta^{2}H$, respectively. For HBL, the range in $\delta^{18}O$ and $\delta^{2}H$ values for all lakes was 10.6‰ (minimum = −12.0‰, maximum = −1.4‰) and 51.5‰ (minimum = −100.3‰, maximum = −48.8‰), respectively, whereas the greatest range for an individual lake in HBL over the 3 year sampling period was much lower (4.7‰ and 20.5‰ for $\delta^{18}O$ and $\delta^{2}H$, respectively). Similarly for NUN, the range in $\delta^{18}O$ and $\delta^{2}H$ values for all lakes was 6.6‰ (minimum = −14.4‰, maximum = −7.8‰) and 35.2‰ (minimum = −107.7, maximum = −72.5), respectively, while the greatest range for an individual lake over multiple years was much lower (2.8‰ and 19.8‰ for $\delta^{18}O$ and $\delta^{2}H$, respectively).

The availability and quality of climate records also varied among the five landscapes, and we used a common gridded climate database to extract meteorological conditions. These data were used to calculate water balance metrics for each individual lake, which allowed for a consistent approach to modeling of all lakes. However, this also added some uncertainty to the model output given that the gridded data set estimates a 30-year average (1961–1990), which was used to represent meteorological conditions during the recent years of actual water sampling. Fortunately, the gridded 30-year averages for humidity were well aligned with sample year humidity, which is a parameter that the isotope-mass balance model is sensitive to. Yet, precipitation during the sampling years was generally higher than the 1961–1990 averages (Fig. 4). Relatively wet conditions may have led to an underestimation of some of the E/I values relative to expected long-term averages, particularly for ACP. Additionally, summer temperature was warmer during the sampling years than the 1961–1990 estimates, with the exception of ACP. Different data sources were used to demarcate catchment vegetation among landscapes (field observations, remote sensing, aerial photographs), which also result in some further uncertainty to comparisons we make below.

Our attempt to develop a consistent modeling approach that could be applied to all lakes and landscapes results in some differences in values presented in this paper compared to the previous landscape-specific studies. For example, estimates of δ_P produced using waterisotopes.org (Bowen 2016) were lower than local precipitation isotope data utilized by Narancic et al. (2017), which placed some lakes in different classifications (snowmelt- versus rainfall-dominated categories). However, both approaches robustly identify that lakes in NUN experience a low degree of evaporation. Assumptions and limitations of data availability were unavoidable, but they are more likely to influence individual lake behaviour than the

large-scale spatial patterns within and among landscapes (the primary aim of this paper), which clearly emerged.

Drivers of hydrological conditions

Meteorological conditions exert a strong influence on water balance of thermokarst lakes (e.g., Riordan et al. 2006; Plug et al. 2008; Labrecque et al. 2009). For temperature and precipitation, mean annual, mean winter, and mean summer values vary greatly among the five landscapes (Fig. 2). Previous water isotope studies of lakes in northern Canada and the continental United States (Gibson and Edwards 2002; Brooks et al. 2014) found that colder regions typically have lower *E*/*I* values compared to warmer regions. This is likely in response to more rapid evaporation at higher temperature and perhaps differences in the length of the open-water season. Variation in ice-out timing within a region due to lake morphometry and among years and regions due to spring temperatures can also strongly affect evaporation season duration (Arp et al. 2015). Based on differences in mean summer temperature of the five landscapes in this study, one might anticipate the lowest *E*/*I* values at ACP and NUN and the highest values at OCF and YF. Indeed, lakes in ACP and NUN have the lowest *E*/*I* values and YF has some of the highest *E*/*I* values, but lakes in OCF have more moderate *E*/*I* values (Fig. 7). However, HBL has a much higher percentage (40%) of lakes with $E/I > 1$ compared to OCF (4%) and YF (30%).

The amount of snowmelt and rainfall input to lakes (direct to the lake surface and via runoff) affects the water balance of thermokarst lakes through the degree of water replenishment that offsets evaporative losses (Schindler and Smol 2006; Bouchard et al. 2013). It may be anticipated that YF has the greatest proportion of lakes with $E/I > 1$, owing to higher temperatures and relatively low mean annual winter and summer precipitation available to offset evaporation. In contrast, NUN was expected to have the lowest *E*/*I* values because it has the lowest mean summer temperature and highest mean winter and summer precipitation. In general, the results are consistent with these expectations; 30% of lakes in YF have *E*/*I* values >1 and 95% of lakes in NUN have *E*/*I* values <0.5. However, HBL, with moderate temperature and precipitation, has the overall greatest proportion of lakes with $E/I > 1$ (40%). Thus, although HBL has the second highest mean annual summer and winter precipitation relative to the other landscapes, precipitation inputs do not offset midsummer evaporative losses for many lakes compared to the other landscapes, evidently even during years of apparent high summer precipitation. Bouchard et al. (2013) came to a similar conclusion that many lakes in HBL do not receive adequate precipitation, particularly snowmelt runoff, to offset midsummer evaporation leading to lake level decline. Snowmelt bypass, which occurs when snowmelt passes through a lake basin while the water mass is still frozen as ice, has been observed in some arctic lakes (e.g., Bergmann and Welch 1985) and may also serve to enhance *E*/*I* ratios in the absence of diluting effects of rainfall (Edwards and McAndrews 1989).

Source waters to lakes in both HBL and ACP were dominated by rainfall at the time of sampling (Fig. 6), but there is a large difference in amount of mean summer precipitation (Fig. 2). Similarly, lakes in OCF, YF, and NUN have snowmelt-dominated source waters, but again, these landscapes differ strongly in their mean winter precipitation. Thus, factors other than seasonal precipitation amounts must play a role in the relative importance of rainfall versus snowmelt inputs to thermokarst lakes in these landscapes. Interestingly, Fig. 2 shows that YF has relatively high temperature and low precipitation compared to the pattern observed for the other landscapes. YF is also the only landscape with lakes with input isotope compositions distinctly characteristic of water from permafrost thaw (Anderson et al. 2013). Higher temperatures since the early 1980s may be promoting more intense permafrost thaw in YF (Anderson et al. 2013). Overall, the data suggest that climate

normals are not the best predictor of hydrological classification of thermokarst lakes when used alone.

Permafrost conditions, which are influenced by climate, affect surface area of thermokarst lakes throughout the Arctic and Subarctic. For example, studies have shown that lake surface area is decreasing in regions of discontinuous permafrost (Yoshikawa and Hinzman 2003; Smith et al. 2005) but expanding in areas of continuous permafrost (Smith et al. 2005). Decreasing lake surface area has largely been attributed to drainage, but increased evaporation in response to climate warming may also play a role (Riordan et al. 2006). The five landscapes in this study span permafrost classifications from sporadic to continuous as well as from water balances indicative of increasing or stable lake water volume ($E/I < 0.5$) to water balances indicative of decreasing lake water volume due to evaporation ($E/I > 1$). E/I values for lakes from the three permafrost categories are highly variable (Table 2; Fig. 8). Lakes in terrain with sporadic permafrost (NUN) have the lowest E/I values, whereas lakes in terrain with discontinuous permafrost (YF, HBL, and NUN) have the highest E/I values. However, lakes from regions classified as having continuous (ACP, OCF, and HBL) and discontinuous (YF, HBL, and NUN) permafrost do have a wide and comparable range of E/I values spanning from close to 0 to greater than 1. Thus, relations among permafrost zones, lake surface area, and lake water balance are not straightforward.

Lake surface area and depth, as imparted by permafrost or other factors, can influence lake water balance. For example, in ACP, Arp et al. (2015) identified that lakes tend to experience longer ice-free seasons if they are shallow enough to have bedfast ice. In YF, Anderson et al. (2013) proposed that lakes with high E/I values are more likely to be relatively shallow. Although specific lake depth measurements were not available for the entire data set in this study, lakes in HBL were by far the shallowest of the five landscapes and, analogous to observations of Anderson et al. (2013) for YF, had the highest E/I ratios.

Of the permafrost categories, lakes located in the discontinuous permafrost zone, where average temperatures are warmer, have the highest proportion classified as evaporation dominated ($E/I > 0.5$) and 25% had $E/I > 1$. This suggests that evaporation in response to climate warming is likely playing an important role in the observed decline of surface area of thermokarst lakes in discontinuous permafrost zones and that lake drainage (lateral or internal) is likely not the sole cause. The dominance of low E/I values (<0.5) in lakes located within the region of sporadic permafrost may be due to ground thaw, which allows increased lateral hydrological connectivity to offset effects of evaporation. Permafrost thaw and the subsequent increased lateral hydrologic connectivity have been shown to maintain positive lake water balances (low E/I values) in Churchill, Manitoba (Wolfe et al. 2011). Overall, E/I results suggest that large-scale predictions of changes in lake area based strictly on permafrost zonation throughout the Arctic and Subarctic likely would not account for the apparent spatial heterogeneity in thermokarst lake hydrological conditions. Additionally, our analysis suggests that lake drainage is not the only cause of lake level decline for thermokarst lakes in discontinuous permafrost zones and that increased evaporation associated with air temperature increase is likely playing an important role in observed water level changes.

Studies from northern regions have suggested that lakes in low-relief, tundra landscapes are more vulnerable to evaporative losses and desiccation than lakes in forested landscapes (e.g., Brock et al. 2009; Turner et al. 2010, 2014; Bouchard et al. 2013). In forested landscapes, taller and denser vegetation entraps greater amounts of wind-redistributed snow than areas of sparse tundra vegetation (Pomeroy et al. 1997; Liston and Sturm 1998; McFadden et al. 2001; Sturm et al. 2001; Brock et al. 2009). In spring, snowmelt runoff to lakes helps to offset evaporative losses throughout the summer. Based on these observations, it could be reasoned that in this study, lakes located in forest-dominant catchments should have lower

Table 2. Results of Kruskal–Wallis tests, which compare evaporation-to-inflow ratios (*E*/*I*) or oxygen isotope composition of lake-specific input water ($\delta^{18}O_I$) values for the different permafrost zones (continuous, discontinuous, and sporadic) and vegetation categories (forest versus tundra dominant).

	χ^2	*P*	df
Permafrost *E*/*I*	60.754	6.417×10^{-14}	2
Vegetation *E*/*I*			
YF	0.702	0.402	1
OCF	3.429	0.064	1
HBL	11.599	0.001	1
NUN	4.811	0.028	1
Vegetation $\delta^{18}O_I$			
YF	3.915	0.048	1
OCF	7.021	0.008	1
HBL	5.951	0.015	1
NUN	4.111	0.043	1

Note: YF, Yukon Flats; OCF, Old Crow Flats; HBL, Hudson Bay Lowlands; NUN, Nunavik.

Fig. 8. Boxplots comparing evaporation-to-inflow ratios (*E*/*I*) for all 376 lakes among permafrost types. The broken line represents *E*/*I* = 0.5, the threshold for evaporation-dominated lakes.

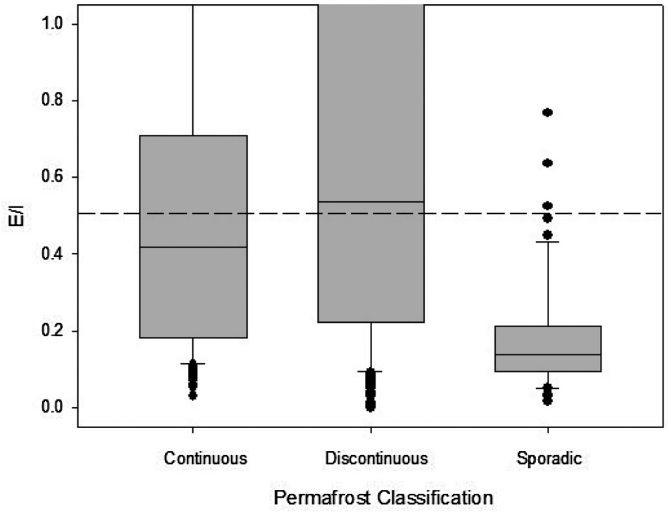

E/*I* and δ_I values than lakes located in tundra-dominant catchments among the five landscapes. Results show that lakes from HBL display the clearest separation of *E*/*I* values between the two catchment vegetation classes with tundra-dominant catchments having higher *E*/*I* values followed by OCF, while lakes from YF have more similar ranges of observed *E*/*I* values for both vegetation classes (Table 2; Fig. 9). Additionally, more lakes in OCF, HBL, and YF have *E*/*I* > 1 in tundra-dominant landscapes compared to lakes situated in forest-dominant catchments. In fact, YF is the only landscape that has forest-dominant lake catchments with *E*/*I* > 1. In contrast, lakes from NUN do not follow this pattern (Fig. 9). Within this landscape, *E*/*I* values span similar albeit low ranges for lakes from both vegetation classes, but *E*/*I* ratios are significantly higher in lakes with forest-dominant catchments compared to lakes with tundra-dominant catchments (Table 2; Fig. 9). For ACP, all *E*/*I* values are relatively low despite that all lakes are situated in tundra-dominant catchments. Results also show that lakes with tundra-dominant catchments in YF, OCF, HBL, and NUN all had higher median $\delta^{18}O_I$ values compared to lakes in these landscapes situated in

Fig. 9. Boxplots comparing evaporation-to-inflow ratios (*E*/*I*, top) and oxygen isotope composition of lake-specific input water ($\delta^{18}O_I$, bottom) for thermokarst lakes at each of the five landscapes between the two vegetation classes (forest versus tundra). The broken line in the upper panel represents *E*/*I* = 0.5, the threshold for evaporation-dominated lakes.

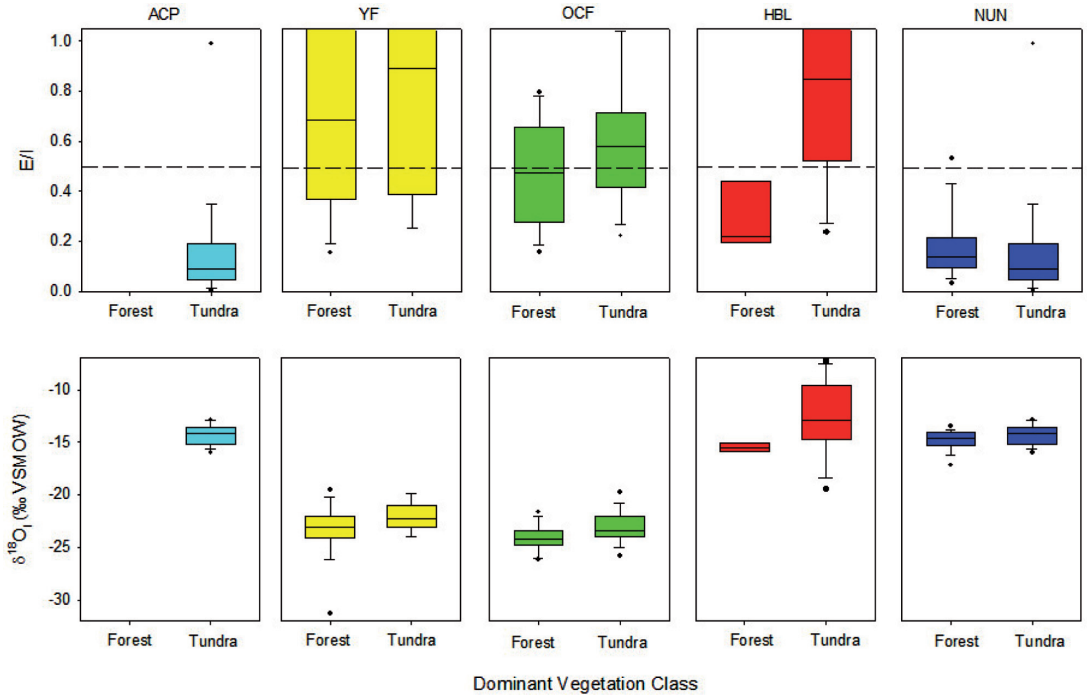

forest-dominant catchments (Table 2; Fig. 9). Thus, tundra-dominant catchments appear to favour greater relative input of rainfall than snowmelt source waters to lakes. Overall, the data suggest that while vegetation appears to influence the composition of thermokarst lake input waters in YF, OCF, HBL, and NUN, the role of vegetation in vapour loss appears to be more important in HBL and OCF, and to a lesser degree in YF, than in NUN.

Interactions among meteorological conditions and catchment characteristics, such as vegetation and permafrost classifications, likely play key roles in promoting the similarities and diversity of hydrological conditions observed among the five landscapes. For example, variability in year-to-year meteorological conditions likely has the ability to mask the expected lake responses to other drivers such as vegetation and permafrost characteristics. ACP lakes all had *E*/*I* values that were relatively low despite all lakes being situated in catchments dominated by tundra vegetation. These values may have been lower than expected due to relatively high rainfall prior to sampling compared to long-term averages (Fig. 4). We speculate that in years of more typical precipitation in ACP, catchment vegetation may play a larger role in thermokarst lake hydrology and *E*/*I* values may be higher and perhaps more comparable to the tundra landscapes observed in HBL, OCF, and YF. Conversely, catchment vegetation may also mediate changes in meteorological conditions. For example, thermokarst lakes in HBL and ACP are mainly rainfall dominated but are also coastal landscapes with the majority of lakes located within open tundra. The coastal tundra settings may promote more wind redistribution of snowfall in these landscapes compared to the more inland snowmelt-dominated landscapes of YF and OCF, perhaps causing the lakes in these tundra landscapes to be more susceptible to hydrological changes in response to yearly fluctuations in rainfall. We further contend that because permafrost and overlying vegetation are influenced by climate conditions, precisely identifying

discrete roles of permafrost and vegetation is difficult. For instance, within a landscape, water balance differences may be due to the climatic conditions that result in vegetation differences rather than caused solely by vegetation. Recognition of the complex interactions and relative importance among different drivers of thermokarst lake hydrology throughout high-latitude regions is required to anticipate future hydrological trajectories (Turner et al. 2014).

Future hydrological trajectories

During the next century, northern regions are expected to experience continued rise of air temperature, longer duration of the ice-free season, and changes in the amount and timing of precipitation (Kattsov et al. 2005; Prowse et al. 2006; AMAP 2011). Increased temperatures and longer ice-free seasons will promote greater vapour loss from lakes during summer (Schindler and Smol 2006; Arp et al. 2015), leading to increased *E*/*I* values. If increases in precipitation do not occur at a similar rate, this could cause widespread desiccation of thermokarst lakes (Bouchard et al. 2013), which has also been observed in shallow non-thermokarst lakes in Canada's High Arctic (Smol and Douglas 2007). Spring snow cover has declined over many areas of northern North America and this pattern is expected to continue, although with substantial spatial and temporal variability (AMAP 2011; Dersken and Brown 2012; Krasting et al. 2013), which may result in a reduction of runoff available for offsetting vapour loss. Thermokarst lakes in HBL have already begun to desiccate during the ice-free season, and analysis of a sediment core from one desiccated lake in HBL indicates that this recent drying trend is unprecedented in the context of the past 200 years (Bouchard et al. 2013). YF, OCF, and perhaps ACP may also evolve towards this scenario under conditions of continued climate warming. Based on the *E*/*I* results of this study, field observations, and the degree to which hydrological conditions in each landscape appear to be influenced by meteorological conditions as outlined above, we suggest that HBL is the most vulnerable of the five landscapes to widespread lake desiccation in the future followed by YF, OCF, and ACP, while NUN is likely the least vulnerable. Interestingly, the landscapes at the two ends of this lake hydrological spectrum lie on opposite sides of Hudson Bay, and this may be related to the more maritime conditions in NUN on the eastern shore (Fig. 2; Narancic et al. 2017).

Increases in shrub growth in response to longer ice-free seasons and warmer temperatures have been observed along tundra–taiga transition zones (Myers-Smith et al. 2011; Lantz et al. 2013). Increased shrub growth may result in an increase in the number of lakes having snowmelt-dominated input waters and, conversely, a decrease in the proportion of rainfall-dominated lakes. This increase may result in greater water replenishment for some lakes in HBL, OCF, YF, and possibly ACP, where tundra-dominated landscapes typically have higher *E*/*I* values. However, the ratio of catchment area to lake size of individual lakes will determine whether sufficient snowmelt runoff can be generated to offset evaporative losses. Furthermore, with more vegetation productivity, increases in terrestrial evapotranspiration may dampen this response.

Greater permafrost thaw throughout high-latitude regions of North America (Osterkamp and Romanovsky 1999; Burn and Kokelj 2009) may result in lake-level declines via increases in vertical lake drainage (e.g., Yoshikawa and Hinzman 2003), or it may result in increased lateral hydrological connectivity, which may offset water losses due to evaporation and vertical drainage, ultimately causing a net increase in lake surface area (Avis et al. 2011; Wolfe et al. 2011). However, previous studies showed that lakes in YF with hydrological connections to the drainage network tend to experience greater fluctuations in intra- and interannual water balances (Chen et al. 2012, 2013). A subset of thermokarst lakes in YF show evidence of source waters derived from permafrost thaw, suggesting that this landscape may be

particularly sensitive to further changes in permafrost. *E*/*I* values of lakes in the sporadic permafrost zone of NUN may also be illustrating the effects of increased hydrological connectivity offsetting vapour loss. As the continuous permafrost warms in ACP, HBL, and OCF, these lakes may also become increasingly influenced by permafrost thaw waters. Overall, thermokarst lakes throughout permafrost regions of North America are unlikely to follow a uniform hydrological trajectory in response to amplified climate change. Rather, the hydrology of thermokarst lakes is likely to display dynamic and individualistic responses depending on their unique set of landscape and climate conditions and drivers.

Conclusions

We compiled water isotope data obtained during the past decade from 376 lakes of mainly thermokarst origin situated in arctic and subarctic permafrost landscapes across North America (Arctic Coastal Plain (Alaska), Yukon Flats (Alaska), Old Crow Flats (Yukon), northwestern Hudson Bay Lowlands (Manitoba), and Nunavik (Quebec)). Our results, as well as those derived from calculation of isotope-based water-balance metrics (including source water isotope compositions and evaporation-to-inflow ratios), demonstrate a substantial array of regional and subregional diversity of lake hydrological conditions characterized by varying influence of snowmelt, rainfall, permafrost thaw waters, and evaporation. Thermokarst lake hydrology is driven by complex interactions among prevailing temperature and precipitation, catchment vegetation, and permafrost status. Some regional patterns emerged, such as the strong role of open-water evaporation on thermokarst lakes of the Hudson Bay Lowlands and Yukon Flats in particular, yet these hydrological drivers are all "moving targets" with ongoing climate change. Thus, they are likely to have pronounced influence on future thermokarst lake hydrological trajectories at a wide range of spatial and temporal scales, challenging our ability to anticipate their consequences for water resources, aquatic ecosystems, and biogeochemical cycling.

Acknowledgements

We would like to thank the many funding agencies and organizations that support our research as well as the many assistants in the field. This is a contribution to the NSERC Discovery Frontiers program, Arctic Development and Adaptation to Permafrost in Transition (ADAPT). Any use of trade, firm, or product names is for descriptive purposes only and does not imply endorsement by the US Government.

References

ACIA. 2004. Arctic climate impact assessment. Cambridge University Press, Cambridge, UK.

Allard, M., and Séguin, M.K. 1987. Le pergélisol au Québec nordique: bilan et perspectives. Géograph. Phys. Quarter. **41**(1): 141–152. doi: 10.7202/032671ar.

Anderson, L., Birks, J., Rover, J., and Guldager, N. 2013. Controls on recent Alaskan lake changes identified from water isotopes and remote sensing. Geophys. Res. Lett. **40**(13): 3413–3418. doi: 10.1002/grl.50672.

Arctic Monitoring and Assessment Programme (AMAP). 2011. Snow, water, ice and permafrost in the Arctic (SWIPA): climate change and the cryosphere. Arctic Monitoring and Assessment Programme, Oslo, Norway.

Arp, C.D., and Jones, B.M. 2009. Geography of Alaska Lake Districts: identification, description, and analysis of lake-rich regions of a diverse and dynamic state. Scientific Investigations Report. US Geological Survey. doi: 10.1002/2015WR017362.

Arp, C.D., Jones, B.M., Liljedahl, A.K., Hinkel, K.M., and Welker, J.A. 2015. Depth, ice thickness, and ice-out timing cause divergent hydrologic responses among Arctic lakes. Water Resour. Res. **51**(12): 9379–9401.

Avis, C.A., Weaver, A.J., and Meissner, K.J. 2011. Reduction in areal extent of high-latitude wetlands in response to permafrost thaw. Nat. Geosci. **4**(7): 444–448. doi: 10.1038/ngeo1160.

Bergmann, M.A., and Welch, W.E. 1985. Spring meltwater mixing in small arctic lakes. Can. J. Fish. Aquat. Sci. **42**(11): 1789–1798. doi: 10.1139/f85-224.

Bouchard, F., Turner, K.W., MacDonald, L.A., Deakin, C., White, H., Farquharson, N., et al. 2013. Vulnerability of shallow subarctic lakes to evaporate and desiccate when snowmelt runoff is low. Geophys. Res. Lett. **40**(23): 6112–6117. doi: 10.1002/2013GL058635.

Bouchard, F., Francus, P., Pienitz, R., Laurion, I., and Feyte, S. 2014. Subarctic thermokarst ponds: investigating recent landscape evolution and sediment dynamics in thawed permafrost of northern Québec (Canada). Arct. Antarct. Alp. Res. **46**(1): 251–271. doi: 10.1657/1938-4246-46.1.251.

Bowen, G.J. 2016. The online isotopes in precipitation calculator, version 2.2. http://www.waterisotopes.org.

Bowen, G.J., Wassenaar, L.I., and Hobson, K.A. 2005. Global application of stable hydrogen and oxygen isotopes to wildlife forensics. Oecologia. **143**(3): 337–348. doi: 10.1007/s00442-004-1813-y.

Brock, B.E., Wolfe, B.B., and Edwards, T.W.D. 2007. Characterizing the hydrology of shallow floodplain lakes in the Slave River Delta, NWT, Canada, using water isotope tracers. Arct. Antarct. Alp. Res. **39**(3): 388–401. doi: 10.1657/1523-0430(06-026)[BROCK]2.0.CO;2.

Brock, B.E., Yi, Y., Clogg-Wright, K.P., Edwards, T.W.D., and Wolfe, B.B. 2009. Multi-year landscape-scale assessment of lakewater balances in the Slave River Delta, NWT, using water isotope tracers. J. Hydrol. **379**(1–2): 81–91. doi: 10.1016/j.jhydrol.2009.09.046.

Brooks, J.R., Gibson, J.J., Birks, S.J., Weber, M.H., Rodecap, K.D., and Stoddard, J.L. 2014. Stable isotope estimates of evaporation: inflow and water residence time for lakes across the United States as a tool for national lake water quality assessments. Limnol. Oceanogr. **59**(6): 2150–2165. doi: 10.4319/lo.2014.59.6.2150.

Brown, J., Ferrians, O., Heginbottom, J.A., and Melnikov, E.S. 2002. Circum-arctic map of permafrost and ground-ice conditions, version 2. NSIDC: National Snow and Ice Data Center/World Data Center for Glaciology, Boulder, CO. http://nsidc.org/data/ggd318 [accessed May 24, 2016].

Burn, C.R., and Kokelj, S.V. 2009. The environment and permafrost of the Mackenzie Delta area. Permafrost Periglacial Process. **20**(2): 83–105. doi: 10.1002/ppp.655.

Carroll, M.L., Townshend, J.R.G., DiMiceli, C.M., Loboda, T., and Sohlberg, R.A. 2011. Shrinking lakes of the Arctic: spatial relationships and trajectory of change. Geophys. Res. Lett. **38**(20): L20406, doi: 10.1029/2011GL049427.

Chen, M., Rowland, J.C., Wilson, C.J., Altmann, G.L., and Brumby, S.P. 2012. Temporal and spatial pattern of thermokarst lake area changes at Yukon Flats, Alaska. Hydrol. Process. **28**(3): 837–852. doi: 10.1002/hyp.9642.

Chen, M., Rowland, J.C., Wilson, C.J., Altmann, G.L., and Brumby, S.P. 2013. The importance of natural variability in lake areas on the detection of permafrost degradation: a case study in the Yukon Flats, Alaska. Permafrost Periglacial Process. **24**(3): 224–240. doi: 10.1002/ppp.1783.

Coplen, T.B. 1996. New guidelines for reporting stable hydrogen, carbon and oxygen isotope ratio data. Geochim. Cosmochim. Acta. **60**(17): 3359–3360. doi: 10.1016/0016-7037(96)00263-3.

Craig, H. 1961. Isotopic variations in meteoric waters. Science. **133**(3465): 1702–1703. doi: 10.1126/science.133.3465.1702.

Craig, H., and Gordon, L.I. 1965. Deuterium and oxygen 18 variations in the ocean and the marine atmosphere. *In* Stable isotopes in oceanographic studies and paleotemperatures. *Edited by* E. Tongiorgi. Laboratorio Di Geologia Nucleare, Pisa, Italy, pp. 9–130.

Darling, G., Bath, A., Gibson, J.J., and Rozanski, K. 2006. Isotopes in water. *In* Isotopes in palaeoenvironmental research. *Edited by* M.J. Leng. Springer, Netherlands. pp. 1–66.

Dersken, C., and Brown, R. 2012. Spring snow cover extent reductions in the 2008–2012 period exceeding climate model projections. Geophys. Res. Lett. **39**(19): L19504.

Duguay, C.R., and Lafleur, P.M. 2003. Determining depth and ice thickness of shallow sub-Arctic lakes using space-borne optical and SAR data. Int. J. Rem. Sens. **24**(3): 475–489. doi: 10.1080/01431160304992.

Edwards, T.W.D., and McAndrews, J.H. 1989. Paleohydrology of a Canadian Shield lake inferred from ^{18}O in sediment cellulose. Can. J. Earth Sci. **26**(9): 1850–1859. doi: 10.1139/e89-158.

Edwards, T.W.D., Wolfe, B.B., Gibson, J.J., and Hammarlund, D. 2004. Use of water isotope tracers in high latitude hydrology and paleohydrology. *In* Long-term environmental change in Arctic and Antarctic lakes. *Edited by* R. Pienitz, M.S.V. Douglas, and J.P. Smol. Springer, Dordrecht. pp. 187–207.

Epstein, S., and Mayeda, T. 1953. Variation of ^{18}O content of waters from natural sources. Geochim. Cosmochim. Acta. **4**(5): 213–224. doi: 10.1016/0016-7037(53)90051-9.

Frohn, R.C., Hinkel, K.M., and Eisner, W.R. 2005. Satellite remote sensing classification of thaw lakes and drained thaw lake basins on the North Slope of Alaska. Rem. Sens. Environ. **97**(1): 116–126. doi: 10.1016/j.rse.2005.04.022.

Gibson, J.J., and Edwards, T.W.D. 2002. Regional water balance trends and evaporation–transpiration partitioning from a stable isotope survey of lakes in northern Canada. Glob. Biogeochem. Cycles. **16**(2): 10-1–10-14.

Gibson, J.J., Birks, S.J., and Edwards, T.W.D. 2008. Global prediction of δ_A and δ^2H–$\delta^{18}O$ evaporation slopes for lakes and soil water accounting for seasonality. Glob. Biogeochem. Cycles. **22**(2): GB2031. doi: 10.1029/2007GB002997.

Gonfiantini, R. 1986. Environmental isotopes in lake studies. *In* Handbook of environmental isotope geochemistry. *Edited by* P. Fritz and J.C. Fontes. Elsevier, New York. pp. 113–168.

Grosse, G., Schirrmeister, L., Kunitsky, V.V., and Hubberten, H.-W. 2005. The use of CORONA images in remote sensing of periglacial geomorphology: an illustration from the NE Siberian coast. Permafrost Periglacial Process. **16**(2): 163–172. doi: 10.1002/ppp.509.

Hinkel, K.M., Jones, B.M., Eisner, W.R., Cuomo, C.J., Beck, R.A., and Frohn, R. 2007. Methods to assess natural and anthropogenic thaw lake drainage on the western Arctic coastal plain of northern Alaska. J. Geophys. Res. **112**(F2): F02S16. doi: 10.1029/2006JF000584.

Horita, J., and Wesolowski, D.J. 1994. Liquid–vapor fractionation of oxygen and hydrogen isotopes of water from the freezing to the critical temperature. Geochim. Cosmochim. Acta. **58**(16): 3425–3437. doi: 10.1016/0016-7037(94)90096-5.

IPCC. 2013. Climate change 2013: the physical science basis. Working Group 1 contribution to the fifth assessment report of the Intergovernmental Panel on Climate Change. *In* IPCC fifth assessment report. *Edited by* T.F. Stocker,

D. Qin, G.-K. Plattner, M.M.B. Tignor, S.K. Allen, J. Boschung, A. Nauels, Y. Xia, V. Bex, and P.M. Midgley. Cambridge University Press, Cambridge, UK.

Jepsen, S.M., Voss, C.I., Walvoord, M.A., Minsley, B.J., and Rover, J. 2013. Linkages between lake shrinkage/expansion and sublacustrine permafrost distribution determined from remote sensing of interior Alaska, USA. Geophys. Res. Lett. **40**(5): 882–887. doi: 10.1002/grl.50187.

Jones, B.M., Grosse, G., Arp, C.D., Jones, M.C., Walter Anthony, K.M., and Romanovsky, V.E. 2011. Modern thermokarst lake dynamics in the continuous permafrost zone, northern Seward Peninsula, Alaska. J. Geophys. Res. **116**(G2): G00M03. doi: 10.1029/2011JG001666.

Kattsov, V.M., Källén, E., Cattle, H., Christensen, J., Drange, H., Hanssen-Bauer, I., Jóhannesen, T., Karol, I., Räisänen, J., et al. 2005. Future climate change: modeling and scenarios for the Arctic. *In* Arctic climate impact assessment. *Edited by* C. Symon, L. Arris, and B. Heal. Cambridge University Press, Cambridge, UK, pp. 99–150.

Krasting, J.P., Broccoli, A.J., Dixon, K.W., and Lanzante, J.R. 2013. Future changes in northern hemisphere snowfall. J. Clim. **26**(20): 7813–7828. doi: 10.1175/JCLI-D-12-00832.1.

Labrecque, S., Lacelle, D., Duguay, C., Lauriol, B., and Hawkings, J. 2009. Contemporary (1951–2001) evolution of lakes in the Old Crow Basin, northern Yukon, Canada: remote sensing, numerical modeling and stable isotope analysis. Arctic. **62**(2): 225–238. doi: 10.14430/arctic134.

Lachniet, M.S., Lawson, D.E., and Sloat, A.R. 2012. Revised ^{14}C dating of ice wedge growth in interior Alaska (USA) to MIS 2 reveals cold paleoclimate and carbon recycling in ancient permafrost terrain. Quat. Res. **78**(2): 217–225. doi: 10.1016/j.yqres.2012.05.007.

Lantz, T.C., Marsh, P., and Kokelj, S.V. 2013. Recent shrub proliferation in the Mackenzie Delta uplands and microclimatic implications. Ecosystems. **16**(1): 47–59. doi: 10.1007/s10021-012-9595-2.

Lauriol, B., Duguay, C.R., and Riel, A. 2002. Response of the Porcupine and Old Crow rivers in northern Yukon, Canada, to Holocene climatic change. Holocene. **12**(1): 27–34. doi: 10.1191/0959683602hl517rp.

Liston, G.E., and Sturm, M. 1998. A snow-transport model for complex terrain. J. Glaciol. **44**(148): 498–516.

MacDonald, L.A., Turner, K.W., Balasubramaniam, A.M., Wolfe, B.B., Hall, R.I., and Sweetman, J.N. 2012. Tracking hydrological responses of a thermokarst lake in the Old Crow Flats (Yukon Territory, Canada) to recent climate variability using aerial photographs and paleolimnological methods. Hydrol. Process. **26**(1): 117–129. doi: 10.1002/hyp.8116.

Mackay, J.R. 1988. Catastrophic lake drainage, Tuktoyaktuk Peninsula area, District of Mackenzie. *In* Current research, part D, geological survey of Canada, paper 88-1D. pp. 83–90.

Marsh, P., Russell, M., Pohl, S., Haywood, H., and Onclin, C. 2009. Changes in thaw lake drainage in the Western Canadian Arctic from 1950 to 2000. Hydrol. Process. **23**(1): 145–158. doi: 10.1002/hyp.7179.

McFadden, J.P., Liston, G.E., Sturm, M., Pielke, R.A., and Chapin, F.S. 2001. Interactions of shrubs and snow in arctic tundra: measurements and models. *In* Soil–vegetation–atmosphere transfer schemes and large-scale hydrological models. *Edited by* A.J. Dolman, A.J. Hall, M.L. Kavvas, T. Oki, and J.W. Pomeroy. International Association of Hydrological Sciences, Wallingford, UK. pp. 317–325.

Meyer, H., Schirrmeister, L., Yoshikawa, K., Opel, T., Wetterich, S., Hubberten, H.-W., and Brown, J. 2010. Permafrost evidence for severe winter cooling during the Younger Dyas in northern Alaska. Geophys. Res. Lett. **37**(3): L03501, doi: 10.1029/2009GL041013.

Morrison, J., Brockwell, T., Merren, T., Fourel, F., and Phillips, A.M. 2001. On-line high-precision stable hydrogen isotopic analyses on nanolitre water samples. Anal. Chem. **73**(15): 3570–3575. doi: 10.1021/ac001447t.

Myers-Smith, I.H., Forbes, B.C., Wilmking, M., Hallinger, M., Lantz, T., Blok, D., et al. 2011. Shrub expansion in tundra ecosystems: dynamics, impacts and research priorities. Environ. Res. Lett. **6**(4): 045509, doi: 10.1088/1748-9326/6/4/045509.

Narancic, B., Wolfe, B.B., Pienitz, R., Meyer, H., and Lamhonwah, D. 2017. Landscape-gradient assessment of thermokarst lake hydrology using water isotope tracers. J. Hydrol. **545**: 327–338. doi: 10.1016/j.jhydrol.2016.11.028.

NARR. 2015. NCEP North American Regional Reanalysis. http://www.esrl.noaa.gov/psd/data/gridded/data.narr.html [accessed winter 2016].

New, M., Lister, D., Hulme, M., and Makin, I. 2002. A high-resolution data set of surface climate over global land areas. Clim. Res. **21**(1): 1–25. http://wcatlas.iwmi.org/Default.asp [accessed fall 2015].

Osterkamp, T.E., and Romanovsky, V.E. 1999. Evidence for warming and thawing of discontinuous permafrost in Alaska. Permafrost Periglacial Process. **10**(1): 17–37. doi: 10.1002/(SICI)1099-1530(199901/03)10:1<17::AID-PPP303>3.0.CO;2-4.

Plug, L.J., Walls, C., and Scott, B.M. 2008. Tundra lake changes from 1978 to 2001 on the Tuktoyaktuk Peninsula, western Canadian Arctic. Geophys. Res. Lett. **35**(3): L03502, doi: 10.1029/2007GL032303.

Pomeroy, J.W., Marsh, P., and Gray, D.M. 1997. Application of a distributed blowing snow model to the Arctic. Hydrol. Process. **11**(11): 1451–1464. doi: 10.1002/(SICI)1099-1085(199709)11:11<1451::AID-HYP449>3.0.CO;2-Q.

Prowse, T.D., Wrona, F.J., Reist, J.D., Gibson, J.J., Hobbie, J.E., Lévesque, L.M., and Vincent, W.F. 2006. Climate change effects on hydroecology of Arctic freshwater ecosystems. Ambio. **35**(7): 347–358. doi: 10.1579/0044-7447(2006)35[347:CCEOHO]2.0.CO;2.

Rampton, V. 1988. Quaternary geology of the Tuktoyaktuk Coastlands, Northwest Territories. Geological Survey of Canada Memoir No. 423.

Riordan, B., Verbyla, D., and McGuire, A.D. 2006. Shrinking ponds in subarctic Alaska based on 1950–2002 remotely sensed images. J. Geophys. Res. **111**(G4): G04002. doi: 10.1029/2005JG000150.

Rouse, W.R. 1991. Impacts of Hudson Bay on the terrestrial climate of the Hudson Bay Lowlands. Arct. Alp. Res. **23**(1): 24–30. doi: 10.2307/1551433.

Rouse, W.R., Douglas, M.S.V., Hecky, R.E., Hershey, A.E., Kling, G.W., Lesack, L., et al. 1997. Effects of climate change on the freshwaters of Arctic and subarctic North America. Hydrol. Process. **11**(8): 873–902. doi: 10.1002/(SICI)1099-1085(19970630)11:8<873::AID-HYP510>3.0.CO;2-6.

Rowland, J.C., Jones, C.E., Altmann, G., Bryan, R., Crosby, B.T., Geernaert, G.L., et al. 2010. Arctic landscapes in transition: responses to thawing permafrost. EOS Trans. Am. Geophys. Union. **91**(26): 229–236. doi: 10.1029/2010EO260001.

Rozanski, K., Araguás-Araguás, L., and Gonfiantini, R. 1993. Isotopic patterns in modern global precipitation. *In* Climate change in continental isotopic records. *Edited by* P.K. Swart, J.A. McKenzie, K.C. Lohmann, and S. Savin. Geophys. Monogr. 78, American Geophyscial Union, Washington, DC. pp. 1–36.

Schindler, D.W., and Smol, J.P. 2006. Cumulative effects of climate warming and other human activities on freshwaters of Arctic and subarctic North America. Ambio. **35**(4): 160–168. doi: 10.1579/0044-7447(2006)35[160:CEOCWA]2.0.CO;2.

Smith, L.C., Sheng, Y., MacDonald, G.M., and Hinzman, L.D. 2005. Disappearing arctic lakes. Science. **308**(5727): 1429. doi: 10.1126/science.1108142.

Smol, J.P., and Douglas, M.S.V. 2007. Crossing the final ecological threshold in high Arctic ponds. Proc. Natl Acad. Sci. U.S.A. **104**(30): 12395–12397. doi: 10.1073/pnas.0702777104.

Sturm, M., McFadden, J.P., Liston, G.E., Chapin, F.S., Racine, C.H., and Holmgren, J. 2001. Snow–shrub interactions in Arctic tundra: a hypothesis with climatic implications. J. Clim. **14**(3): 336–344. doi: 10.1175/1520-0442(2001)014<0336:SSIIAT>2.0.CO;2.

Thornthwaite, C. 1948. An approach toward a rational classification of climate. Geogr. Rev. **38**(1): 55–94. doi: 10.2307/210739.

Tondu, J.M.E., Turner, K.W., Wolfe, B.B., Hall, R.I., Edwards, T.W.D., and McDonald, I. 2013. Using water isotope tracers to develop the hydrological component of a long-term aquatic ecosystem monitoring program for a northern lake-rich landscape. Arct. Antarct. Alp. Res. **45**(4): 594–614. doi: 10.1657/1938-4246-45.4.594.

Tranvik, L.J., Downing, J.A., Cotner, J.B., Loiselle, S.A., Striegl, R.G., Ballatore, T.J., et al. 2009. Lakes and reservoirs as regulators of carbon cycling and climate. Limnol. Oceanogr. **54**(6): 2298–2314. doi: 10.4319/lo.2009.54.6_part_2.2298.

Turner, K.W., Wolfe, B.B., and Edwards, T.W.D. 2010. Characterizing the role of hydrological processes on lake water balances in the Old Crow Flats, Yukon Territory, Canada, using water isotope tracers. J. Hydrol. **386**(1–4): 103–117. doi: 10.1016/j.jhydrol.2010.03.012.

Turner, K.W., Wolfe, B.W., Edwards, T.W.D., Lantz, T.C., Hall, R.I., and Larocque, G. 2014. Controls on water balance of shallow thermokarst lakes and their relations with catchment characteristics: a multi-year, landscape-scale assessment based on water isotope tracers and remote sensing in Old Crow Flats, Yukon (Canada). Glob. Change Biol. **20**(5): 1585–1603. doi: 10.1111/gcb.12465.

Vincent, W.F., Lemay, M., Allard, M., and Wolfe, B.B. 2013. Adapting to permafrost change: a science framework. Brief report. EOS. **94**(42): 373–375. doi: 10.1002/2013EO420002.

Williams, J.R. 1962. Geologic reconnaissance of the Yukon Flats district, Alaska. U.S. Geol. Surv. Bull. **1111-H**: H289–H331.

Wolfe, B.B., Light, E.M., Macrae, M.L., Hall, R.I., Eichel, K., Jasechko, S., et al. 2011. Divergent hydrological responses to 20th century climate change in shallow tundra ponds, western Hudson Bay Lowlands. Geophys. Res. Lett. **38**(23): L23402, doi: 10.1029/2011GL049766.

Yi, Y., Brock, B.E., Falcone, M.D., Wolfe, B.B., and Edwards, T.W.D. 2008. A coupled isotope tracer method to characterize input water to lakes. J. Hydrol. **350**(1–2): 1–13. doi: 10.1016/j.jhydrol.2007.11.008.

Yoshikawa, K.S., and Hinzman, L.D. 2003. Shrinking thermokarst ponds and groundwater dynamics in discontinuous permafrost near Council, Alaska. Permafrost Periglacial Process. **14**(2): 151–160. doi: 10.1002/ppp.451.

Appendix

Table A1. Average summer water isotope compositions, coordinates, and vegetation and permafrost categories for each of the 376 lakes.

Lake	δ_L (^{18}O)	δ_L (^{2}H)	Latitude (° N)	Longitude (° W)	Vegetation	Permafrost
ACP1	–9.26	–80.20	70.752	–153.869	Tundra	Continuous
ACP2	–12.34	–97.92	70.766	–153.562	Tundra	Continuous
ACP3	–10.55	–87.84	70.789	–153.470	Tundra	Continuous
ACP4	–14.72	–114.15	70.790	–154.450	Tundra	Continuous
ACP5	–11.74	–95.53	70.793	–154.517	Tundra	Continuous
ACP6	–12.95	–102.04	70.706	–153.924	Tundra	Continuous
ACP7	–12.07	–98.70	70.361	–151.683	Tundra	Continuous
ACP8	–15.25	–119.47	70.367	–151.398	Tundra	Continuous
ACP9	–16.26	–129.62	70.321	–151.532	Tundra	Continuous
ACP10	–14.55	–116.74	70.308	–151.435	Tundra	Continuous
ACP11	–16.65	–129.27	70.299	–151.464	Tundra	Continuous
ACP12	–13.90	–110.61	70.265	–151.394	Tundra	Continuous
ACP13	–12.65	–110.53	70.270	–151.356	Tundra	Continuous
ACP14	–13.66	–109.73	70.246	–153.287	Tundra	Continuous
ACP15	–11.06	–96.07	70.248	–151.484	Tundra	Continuous
ACP16	–12.64	–108.11	70.253	–151.342	Tundra	Continuous
ACP17	–14.60	–114.59	70.229	–153.312	Tundra	Continuous
ACP18	–13.03	–114.18	70.218	–153.179	Tundra	Continuous
ACP19	–13.86	–115.03	70.230	–153.090	Tundra	Continuous
ACP20	–12.98	–106.65	70.231	–151.367	Tundra	Continuous
ACP21	–13.55	–110.14	70.208	–151.169	Tundra	Continuous
ACP22	–13.95	–114.54	70.198	–153.315	Tundra	Continuous
ACP23	–12.29	–103.76	70.214	–153.313	Tundra	Continuous
ACP24	–12.72	–110.64	70.213	–153.082	Tundra	Continuous
ACP25	–13.18	–109.87	70.204	–152.566	Tundra	Continuous
ACP26	–13.21	–110.17	70.179	–153.294	Tundra	Continuous
ACP27	–12.99	–108.00	70.187	–151.571	Tundra	Continuous
ACP28	–14.66	–121.73	70.146	–151.761	Tundra	Continuous
ACP29	–14.12	–118.35	70.129	–151.804	Tundra	Continuous
ACP30	–14.01	–114.25	70.097	–152.880	Tundra	Continuous
ACP31	–13.41	–118.04	70.068	–152.962	Tundra	Continuous
ACP32	–14.24	–118.47	70.035	–153.288	Tundra	Continuous
ACP33	–15.12	–120.13	70.035	–153.227	Tundra	Continuous
ACP34	–14.23	–114.72	70.035	–153.039	Tundra	Continuous
ACP35	–17.01	–135.16	70.018	–153.188	Tundra	Continuous
ACP36	–18.54	–142.04	70.012	–153.153	Tundra	Continuous
ACP37	–14.30	–119.44	70.012	–153.094	Tundra	Continuous
ACP38	–13.56	–110.80	70.000	–152.028	Tundra	Continuous
ACP39	–14.99	–121.29	69.997	–153.069	Tundra	Continuous
ACP40	–11.77	–104.34	70.000	–153.037	Tundra	Continuous
ACP41	–15.13	–122.04	69.979	–153.074	Tundra	Continuous
ACP42	–14.14	–114.37	69.969	–152.946	Tundra	Continuous
ACP43	–11.93	–112.28	69.992	–152.952	Tundra	Continuous
ACP44	–15.37	–125.56	69.659	–153.051	Tundra	Continuous
YF1	–7.90	–100.73	66.450	–145.546	Forest	Discontinuous
YF2	–4.46	–84.94	66.450	–145.563	Forest	Discontinuous
YF3	–13.04	–129.30	66.385	–146.360	Forest	Discontinuous
YF4	–12.89	–125.86	66.034	–147.544	Forest	Discontinuous

Table A1 (*continued*).

Lake	δ_L (^{18}O)	δ_L (^{2}H)	Latitude (° N)	Longitude (° W)	Vegetation	Permafrost
YF5	–9.04	–106.11	66.294	–148.114	Forest	Discontinuous
YF6	–8.97	–106.40	66.088	–146.733	Forest	Discontinuous
YF7	–9.49	–109.35	66.240	–146.394	Forest	Discontinuous
YF8	–10.02	–112.15	66.083	–146.316	Forest	Discontinuous
YF9	–11.68	–120.00	66.175	–146.144	Forest	Discontinuous
YF10	–14.77	–136.61	66.186	–147.493	Forest	Discontinuous
YF11	–16.49	–144.37	65.929	–146.596	Forest	Discontinuous
YF12	–10.50	–116.86	66.129	–146.660	Forest	Discontinuous
YF13	–18.00	–155.82	66.282	–149.321	Forest	Discontinuous
YF14	–9.98	–111.39	66.259	–148.935	Forest	Discontinuous
YF15	–15.14	–141.79	66.337	–148.984	Forest	Discontinuous
YF16	–15.22	–142.46	66.240	–148.825	Forest	Discontinuous
YF17	–17.59	–150.50	66.229	–146.943	Forest	Discontinuous
YF18	–9.91	–116.08	66.223	–146.688	Forest	Discontinuous
YF19	–13.58	–135.62	66.217	–146.417	Forest	Discontinuous
YF20	–10.54	–118.78	66.217	–146.385	Forest	Discontinuous
YF21	–8.77	–112.11	66.258	–146.331	Forest	Discontinuous
YF22	–10.52	–116.84	66.320	–146.320	Forest	Discontinuous
YF23	–12.00	–127.86	66.299	–146.187	Forest	Discontinuous
YF24	–18.29	–158.00	66.106	–148.220	Forest	Discontinuous
YF25	–9.17	–109.27	66.171	–147.975	Forest	Discontinuous
YF26	–18.21	–156.04	66.208	–147.669	Forest	Discontinuous
YF27	–11.20	–121.94	66.067	–149.327	Forest	Discontinuous
YF28	–14.50	–139.92	66.117	–149.069	Forest	Discontinuous
YF29	–7.76	–104.12	66.200	–148.682	Forest	Discontinuous
YF30	–9.13	–111.44	66.459	–147.903	Forest	Discontinuous
YF31	–8.40	–105.14	66.389	–147.573	Forest	Discontinuous
YF32	–7.37	–103.30	66.430	–147.412	Forest	Discontinuous
YF33	–17.43	–152.56	66.055	–146.384	Forest	Discontinuous
YF34	–14.16	–137.52	66.061	–145.782	Forest	Discontinuous
YF35	–13.72	–136.30	66.187	–145.668	Forest	Discontinuous
YF36	–18.51	–158.26	66.207	–145.658	Forest	Discontinuous
YF37	–18.70	–158.91	66.277	–145.708	Forest	Discontinuous
YF38	–14.53	–139.24	66.110	–145.561	Forest	Discontinuous
YF39	–11.48	–122.97	66.368	–145.562	Forest	Discontinuous
YF40	–18.85	–153.56	66.185	–145.444	Forest	Discontinuous
YF41	–15.41	–143.52	66.010	–146.444	Forest	Discontinuous
YF42	–18.63	–156.95	65.999	–146.468	Forest	Discontinuous
YF43	–10.44	–117.81	66.281	–148.593	Forest	Discontinuous
YF44	–12.87	–130.87	66.327	–148.595	Forest	Discontinuous
YF45	–9.70	–115.61	66.275	–148.221	Forest	Discontinuous
YF46	–10.03	–115.81	66.307	–148.102	Forest	Discontinuous
YF47	–10.30	–118.18	66.314	–148.106	Forest	Discontinuous
YF48	–10.18	–115.71	66.280	–148.120	Forest	Discontinuous
YF49	–11.30	–120.90	66.123	–148.153	Forest	Discontinuous
YF50	–18.80	–156.90	66.131	–149.159	Forest	Discontinuous
YF51	–16.90	–162.50	65.971	–149.450	Forest	Discontinuous
YF52	–11.60	–128.70	66.167	–149.159	Forest	Discontinuous
YF53	–17.30	–165.70	66.260	–148.878	Forest	Discontinuous
YF54	–7.40	–105.50	66.179	–148.989	Forest	Discontinuous
YF55	–10.40	–110.00	66.106	–147.554	Forest	Discontinuous

Table A1 (*continued*).

Lake	δ_L (^{18}O)	δ_L (^{2}H)	Latitude (° N)	Longitude (° W)	Vegetation	Permafrost
YF56	–13.20	–125.00	66.110	–147.753	Forest	Discontinuous
YF57	–11.90	–139.00	66.150	–147.731	Forest	Discontinuous
YF58	–9.20	–105.00	66.181	–148.010	Forest	Discontinuous
YF59	–16.10	–153.00	66.110	–148.313	Forest	Discontinuous
YF60	–16.70	–149.00	66.993	–146.169	Forest	Discontinuous
YF61	–10.30	–119.00	66.983	–146.041	Forest	Discontinuous
YF62	–10.70	–117.00	66.928	–146.125	Forest	Discontinuous
YF63	–19.10	–160.00	66.783	–145.799	Forest	Discontinuous
YF64	–10.40	–113.00	66.909	–145.113	Forest	Discontinuous
YF65	–10.50	–115.00	66.897	–145.170	Forest	Discontinuous
YF66	–7.20	–99.00	66.856	–145.170	Forest	Discontinuous
YF67	–7.30	–98.00	66.775	–145.258	Forest	Discontinuous
YF68	–12.90	–127.00	66.751	–145.458	Forest	Discontinuous
YF69	–12.10	–124.00	66.707	–145.530	Forest	Discontinuous
YF70	–16.70	–145.00	66.154	–144.118	Forest	Discontinuous
YF71	–14.50	–137.00	66.752	–143.502	Forest	Discontinuous
YF72	–10.50	–116.00	66.716	–143.673	Forest	Discontinuous
YF73	–18.90	–157.00	66.444	–144.384	Forest	Discontinuous
YF74	–10.80	–119.00	66.418	–145.368	Forest	Discontinuous
YF75	–7.80	–113.60	66.101	–146.007	Forest	Discontinuous
YF76	–7.90	–113.60	66.625	–146.234	Forest	Discontinuous
YF77	–7.80	–118.40	66.269	–145.902	Forest	Discontinuous
YF78	–6.80	–114.60	66.867	–143.837	Forest	Discontinuous
YF79	–8.00	–117.60	66.871	–143.829	Forest	Discontinuous
YF80	–10.30	–129.90	66.995	–143.749	Forest	Discontinuous
YF81	–13.70	–146.30	66.977	–143.327	Forest	Discontinuous
YF82	–8.30	–116.70	66.796	–143.538	Forest	Discontinuous
YF83	–8.60	–121.30	66.657	–143.839	Forest	Discontinuous
YF84	–8.44	–104.57	66.401	–146.384	Forest	Discontinuous
YF85	–13.78	–130.33	66.087	–146.729	Forest	Discontinuous
YF86	–6.95	–98.55	66.440	–145.477	Forest	Discontinuous
YF87	–6.74	–100.34	66.437	–145.479	Forest	Discontinuous
YF88	–5.61	–98.87	66.431	–145.536	Forest	Discontinuous
YF89	–15.87	–145.37	66.391	–148.325	Forest	Discontinuous
YF90	–8.48	–110.57	66.386	–148.344	Forest	Discontinuous
YF91	–15.87	–146.01	66.385	–148.328	Forest	Discontinuous
YF92	–17.16	–149.19	66.386	–148.321	Forest	Discontinuous
YF93	–7.66	–107.94	66.387	–148.304	Forest	Discontinuous
YF94	–8.05	–106.63	66.386	–148.290	Forest	Discontinuous
YF95	–15.51	–144.20	66.383	–148.317	Forest	Discontinuous
YF96	–10.91	–126.72	66.384	–148.350	Forest	Discontinuous
YF97	–6.93	–106.47	66.383	–148.355	Forest	Discontinuous
YF98	–12.11	–125.30	66.376	–148.348	Forest	Discontinuous
YF99	–10.17	–115.23	66.371	–148.312	Forest	Discontinuous
YF100	–11.68	–124.20	66.373	–148.350	Forest	Discontinuous
YF101	–12.03	–126.97	66.367	–148.324	Forest	Discontinuous
YF102	–6.68	–106.88	66.388	–148.298	Forest	Discontinuous
YF103	–9.15	–106.96	66.120	–148.048	Forest	Discontinuous
YF104	–12.98	–131.12	66.106	–148.076	Forest	Discontinuous
YF105	–19.29	–158.25	66.109	–148.089	Forest	Discontinuous
YF106	–19.91	–160.80	66.111	–148.050	Forest	Discontinuous

Table A1 (*continued*).

Lake	δ_L (^{18}O)	δ_L (^{2}H)	Latitude (° N)	Longitude (° W)	Vegetation	Permafrost
YF107	–16.01	–143.73	66.109	–148.056	Forest	Discontinuous
YF108	–18.68	–155.32	66.106	–148.089	Forest	Discontinuous
YF109	–12.31	–131.50	66.105	–148.071	Forest	Discontinuous
YF110	–18.20	–154.12	66.105	–148.056	Forest	Discontinuous
YF111	–17.05	–149.82	66.101	–148.097	Forest	Discontinuous
YF112	–18.53	–154.64	66.102	–148.093	Forest	Discontinuous
YF113	–13.04	–132.20	66.102	–148.079	Forest	Discontinuous
YF114	–17.59	–150.68	66.100	–148.100	Forest	Discontinuous
YF115	–13.61	–131.44	66.091	–148.077	Forest	Discontinuous
YF116	–19.32	–158.10	66.098	–148.097	Forest	Discontinuous
YF117	–17.72	–151.41	66.100	–148.090	Forest	Discontinuous
YF118	–17.95	–151.18	66.097	–148.087	Forest	Discontinuous
YF119	–17.33	–150.48	66.093	–148.057	Forest	Discontinuous
YF120	–11.03	–119.80	66.119	–148.063	Forest	Discontinuous
YF121	–11.06	–120.61	66.030	–144.742	Forest	Discontinuous
YF122	–15.21	–141.09	66.029	–144.737	Forest	Discontinuous
YF123	–16.08	–143.84	66.026	–144.727	Forest	Discontinuous
YF124	–19.66	–152.93	66.015	–144.728	Forest	Discontinuous
YF125	–11.84	–124.03	66.017	–144.780	Forest	Discontinuous
YF126	–13.85	–133.63	66.015	–144.769	Forest	Discontinuous
YF127	–12.13	–124.71	66.013	–144.773	Forest	Discontinuous
YF128	–13.64	–132.99	66.012	–144.781	Forest	Discontinuous
YF129	–9.16	–112.63	66.010	–144.783	Forest	Discontinuous
YF130	–15.09	–138.96	66.010	–144.759	Forest	Discontinuous
YF131	–16.66	–144.47	66.014	–144.739	Forest	Discontinuous
YF132	–11.05	–121.14	66.006	–144.769	Forest	Discontinuous
YF133	–15.38	–141.68	66.008	–144.743	Forest	Discontinuous
YF134	–16.78	–147.14	66.008	–144.739	Forest	Discontinuous
YF135	–19.03	–151.79	66.007	–144.735	Forest	Discontinuous
YF136	–15.33	–140.60	66.011	–144.748	Tundra	Discontinuous
YF137	–7.23	–102.70	66.359	–144.268	Tundra	Discontinuous
YF138	–8.86	–108.58	66.364	–144.253	Tundra	Discontinuous
YF139	–13.94	–131.38	66.361	–144.265	Tundra	Discontinuous
YF140	–17.14	–139.55	66.366	–144.233	Tundra	Discontinuous
YF141	–13.09	–129.97	66.359	–144.237	Tundra	Discontinuous
YF142	–7.06	–101.11	66.362	–144.225	Tundra	Discontinuous
YF143	–11.29	–122.05	66.355	–144.232	Tundra	Discontinuous
YF144	–15.52	–142.31	66.358	–144.250	Tundra	Discontinuous
YF145	–14.83	–136.58	66.359	–144.241	Tundra	Discontinuous
YF146	–8.68	–106.50	66.400	–146.371	Tundra	Discontinuous
YF147	–11.73	–126.31	66.397	–146.409	Tundra	Discontinuous
YF148	–10.13	–117.17	66.396	–146.355	Tundra	Discontinuous
YF149	–8.33	–103.76	66.386	–146.367	Tundra	Discontinuous
OCF1	–12.80	–129.03	68.077	–140.110	Forest	Continuous
OCF2	–12.31	–123.44	68.202	–140.296	Tundra	Continuous
OCF3	–16.85	–153.07	68.214	–140.097	Tundra	Continuous
OCF4	–12.67	–128.04	68.215	–140.134	Tundra	Continuous
OCF5	–12.90	–130.77	68.207	–139.884	Forest	Continuous
OCF6	–9.55	–109.56	67.919	–139.991	Tundra	Continuous
OCF7	–17.08	–151.61	67.921	–140.150	Forest	Continuous
OCF8	–14.16	–137.22	67.907	–140.124	Forest	Continuous

Table A1 (*continued*).

Lake	δ_L (^{18}O)	δ_L (^{2}H)	Latitude (° N)	Longitude (° W)	Vegetation	Permafrost
OCF9	–14.34	–137.44	67.906	–140.205	Forest	Continuous
OCF10	–14.70	–140.38	67.891	–140.235	Forest	Continuous
OCF11	–16.92	–155.19	68.028	–140.570	Forest	Continuous
OCF12	–12.60	–130.32	68.061	–140.411	Tundra	Continuous
OCF13	–20.21	–168.70	68.059	–140.364	Forest	Continuous
OCF14	–12.80	–129.64	67.977	–140.234	Forest	Continuous
OCF15	–13.51	–133.98	68.107	–140.674	Tundra	Continuous
OCF16	–19.58	–164.33	68.152	–140.893	Tundra	Continuous
OCF17	–15.37	–147.36	68.229	–140.735	Tundra	Continuous
OCF18	–11.79	–124.93	68.267	–140.619	Tundra	Continuous
OCF19	–12.04	–126.71	68.283	–140.522	Tundra	Continuous
OCF20	–14.17	–138.55	68.185	–140.444	Forest	Continuous
OCF21	–16.92	–152.17	67.739	–140.180	Forest	Continuous
OCF22	–15.76	–148.79	67.764	–140.152	Forest	Continuous
OCF23	–16.44	–152.50	67.765	–140.154	Forest	Continuous
OCF24	–13.44	–133.86	67.771	–140.049	Tundra	Continuous
OCF25	–19.18	–162.83	67.806	–140.055	Forest	Continuous
OCF26	–17.63	–154.29	67.848	–139.992	Forest	Continuous
OCF27	–12.81	–127.87	68.004	–140.052	Forest	Continuous
OCF28	–12.77	–126.14	67.962	–139.898	Forest	Continuous
OCF29	–13.13	–126.92	67.911	–139.794	Tundra	Continuous
OCF30	–14.01	–135.94	67.958	–139.781	Tundra	Continuous
OCF31	–15.00	–141.60	67.961	–139.787	Tundra	Continuous
OCF32	–20.46	–166.84	67.731	–139.615	Forest	Continuous
OCF33	–14.30	–135.53	67.810	–139.461	Tundra	Continuous
OCF34	–14.30	–134.33	67.884	–139.472	Tundra	Continuous
OCF35	–14.48	–137.73	67.979	–139.620	Tundra	Continuous
OCF36	–12.98	–128.15	68.015	–139.712	Tundra	Continuous
OCF37	–12.69	–126.97	68.044	–139.806	Forest	Continuous
OCF38	–14.58	–135.37	68.322	–140.129	Tundra	Continuous
OCF39	–12.64	–124.70	68.337	–140.367	Tundra	Continuous
OCF40	–15.69	–141.70	67.710	–139.432	Forest	Continuous
OCF41	–15.77	–144.69	67.726	–139.083	Tundra	Continuous
OCF42	–14.08	–127.90	67.865	–139.206	Tundra	Continuous
OCF43	–15.53	–140.36	68.036	–139.047	Tundra	Continuous
OCF44	–16.15	–144.14	68.103	–139.185	Tundra	Continuous
OCF45	–18.62	–160.83	68.231	–139.483	Tundra	Continuous
OCF46	–12.49	–128.87	68.150	–139.606	Tundra	Continuous
OCF47	–13.23	–134.00	68.205	–139.808	Forest	Continuous
OCF48	–18.76	–158.88	68.192	–139.879	Forest	Continuous
OCF49	–12.58	–126.60	68.082	–139.662	Tundra	Continuous
OCF50	–19.48	–163.04	67.772	–139.919	Forest	Continuous
OCF51	–17.86	–156.10	67.829	–139.823	Forest	Continuous
OCF52	–17.72	–157.39	67.843	–139.808	Forest	Continuous
OCF53	–13.75	–135.25	67.848	–139.777	Forest	Continuous
OCF54	–18.56	–159.53	67.931	–139.671	Tundra	Continuous
OCF55	–20.05	–168.60	67.843	–139.758	Forest	Continuous
OCF56	–18.55	–159.93	67.812	–139.937	Forest	Continuous
OCF57	–14.88	–139.46	68.208	–139.807	Forest	Continuous
HBL1	–10.67	–91.20	58.394	–93.382	Tundra	Continuous
HBL2	–6.63	–73.46	58.385	–93.345	Tundra	Continuous

Table A1 (*continued*).

Lake	δ_L (^{18}O)	δ_L (^{2}H)	Latitude (° N)	Longitude (° W)	Vegetation	Permafrost
HBL3	–2.85	–55.15	58.343	–93.271	Tundra	Continuous
HBL4	–4.83	–63.97	58.341	–93.268	Tundra	Continuous
HBL5	–5.75	–68.19	58.342	–93.265	Tundra	Continuous
HBL6	–5.70	–66.41	58.351	–93.232	Tundra	Continuous
HBL7	–7.60	–72.99	58.427	–93.178	Tundra	Continuous
HBL8	–7.46	–73.42	58.406	–93.264	Tundra	Continuous
HBL9	–6.65	–69.59	58.414	–93.307	Tundra	Continuous
HBL10	–5.86	–63.15	58.425	–93.268	Tundra	Continuous
HBL11	–5.66	–62.22	58.425	–93.266	Tundra	Continuous
HBL12	–3.89	–59.10	58.426	–93.269	Tundra	Continuous
HBL13	–8.91	–77.42	58.660	–93.194	Tundra	Continuous
HBL14	–7.47	–73.07	58.621	–93.174	Tundra	Continuous
HBL15	–8.02	–73.32	58.620	–93.171	Tundra	Continuous
HBL16	–9.32	–84.81	58.541	–93.161	Tundra	Continuous
HBL17	–7.51	–72.45	58.561	–93.167	Tundra	Continuous
HBL18	–6.90	–70.03	58.622	–93.318	Tundra	Continuous
HBL19	–6.95	–67.95	58.707	–93.299	Tundra	Continuous
HBL20	–7.41	–73.21	58.670	–93.444	Tundra	Continuous
HBL21	–5.86	–68.52	58.665	–93.441	Tundra	Continuous
HBL22	–9.94	–84.83	57.963	–94.077	Tundra	Discontinuous
HBL23	–10.12	–91.34	57.835	–94.183	Forest	Discontinuous
HBL24	–11.52	–95.78	57.739	–94.005	Forest	Discontinuous
HBL25	–11.29	–95.31	57.705	–94.046	Forest	Discontinuous
HBL26	–11.75	–98.23	57.698	–94.115	Forest	Discontinuous
HBL27	–11.52	–97.31	57.614	–93.970	Forest	Discontinuous
HBL28	–10.03	–92.44	57.661	–93.924	Forest	Discontinuous
HBL29	–8.59	–83.16	57.673	–93.432	Tundra	Continuous
HBL30	–3.45	–54.37	57.712	–93.383	Tundra	Continuous
HBL31	–2.40	–53.04	57.737	–93.377	Tundra	Continuous
HBL32	–4.93	–64.66	57.990	–93.459	Tundra	Continuous
HBL33	–8.25	–78.05	58.052	–93.533	Tundra	Continuous
HBL34	–6.43	–71.65	58.046	–93.659	Tundra	Continuous
HBL35	–6.07	–70.97	58.045	–93.659	Tundra	Continuous
HBL36	–8.93	–82.02	58.046	–93.660	Tundra	Continuous
HBL37	–8.53	–81.98	58.078	–93.661	Tundra	Continuous
HBL38	–8.69	–80.82	58.119	–93.554	Tundra	Continuous
HBL39	–10.67	–89.71	58.215	–93.708	Tundra	Continuous
HBL40	–9.91	–86.15	58.365	–93.777	Tundra	Continuous
NUN1	–12.18	–95.12	55.220	–77.707	Forest	Sporadic
NUN2	–12.81	–97.50	55.220	–77.707	Forest	Sporadic
NUN3	–12.46	–98.40	55.227	–77.696	Forest	Sporadic
NUN4	–12.38	–96.27	55.227	–77.698	Forest	Sporadic
NUN5	–12.13	–94.57	55.226	–77.698	Forest	Sporadic
NUN6	–12.09	–93.48	55.227	–77.698	Forest	Sporadic
NUN7	–13.22	–99.10	55.227	–77.698	Forest	Sporadic
NUN8	–11.97	–93.55	55.227	–77.696	Forest	Sporadic
NUN9	–12.42	–97.43	55.223	–77.706	Forest	Sporadic
NUN10	–11.86	–96.64	55.223	–77.706	Forest	Sporadic
NUN11	–12.46	–97.55	55.223	–77.706	Forest	Sporadic
NUN12	–12.25	–94.16	55.227	–77.697	Forest	Sporadic
NUN13	–12.75	–95.10	55.227	–77.697	Forest	Sporadic

Table A1 (*continued*).

Lake	δ_L (^{18}O)	δ_L (^{2}H)	Latitude (° N)	Longitude (° W)	Vegetation	Permafrost
NUN14	–11.67	–90.93	55.227	–77.696	Forest	Sporadic
NUN15	–12.72	–93.49	55.227	–77.698	Forest	Sporadic
NUN16	–11.93	–93.14	55.226	–77.698	Forest	Sporadic
NUN17	–12.59	–95.46	55.227	–77.698	Forest	Sporadic
NUN18	–12.81	–95.75	55.227	–77.698	Forest	Sporadic
NUN19	–12.73	–96.65	55.227	–77.696	Forest	Sporadic
NUN20	–10.40	–83.96	55.222	–77.706	Forest	Sporadic
NUN21	–11.01	–87.90	55.222	–77.706	Forest	Sporadic
NUN22	–11.55	–88.73	55.222	–77.706	Forest	Sporadic
NUN23	–11.61	–92.29	55.331	–77.503	Forest	Sporadic
NUN24	–11.32	–91.57	55.497	–77.503	Forest	Sporadic
NUN25	–11.82	–95.10	55.331	–77.503	Forest	Sporadic
NUN26	–10.23	–87.77	55.332	–77.503	Forest	Sporadic
NUN27	–11.98	–94.43	55.332	–77.502	Forest	Sporadic
NUN28	–8.47	–77.76	55.332	–77.502	Forest	Sporadic
NUN29	–10.53	–87.83	55.332	–77.501	Forest	Sporadic
NUN30	–11.54	–92.67	55.332	–77.502	Forest	Sporadic
NUN31	–8.83	–82.03	55.333	–77.500	Forest	Sporadic
NUN32	–9.70	–85.52	55.330	–77.503	Forest	Sporadic
NUN33	–11.57	–90.98	55.330	–77.504	Forest	Sporadic
NUN34	–11.09	–88.58	55.330	–77.504	Forest	Sporadic
NUN35	–9.45	–84.41	55.330	–77.503	Forest	Sporadic
NUN36	–9.76	–87.49	55.330	–77.502	Forest	Sporadic
NUN37	–10.97	–87.66	55.330	–77.503	Forest	Sporadic
NUN38	–10.92	–89.17	55.330	–77.503	Forest	Sporadic
NUN39	–9.09	–80.61	55.330	–77.505	Forest	Sporadic
NUN40	–10.73	–88.97	55.330	–77.504	Forest	Sporadic
NUN41	–10.93	–91.55	55.332	–77.502	Forest	Sporadic
NUN42	–11.50	–91.85	55.332	–77.503	Forest	Sporadic
NUN43	–11.58	–90.90	55.333	–77.502	Forest	Sporadic
NUN44	–9.82	–85.07	55.333	–77.502	Forest	Sporadic
NUN45	–11.42	–93.62	55.333	–77.502	Forest	Sporadic
NUN46	–11.15	–89.27	55.332	–77.502	Forest	Sporadic
NUN47	–11.46	–92.98	55.332	–77.503	Forest	Sporadic
NUN48	–11.55	–92.55	55.332	–77.503	Forest	Sporadic
NUN49	–10.66	–88.06	55.333	–77.501	Forest	Sporadic
NUN50	–10.03	–85.60	55.332	–77.500	Forest	Sporadic
NUN51	–11.06	–90.50	55.332	–77.501	Forest	Sporadic
NUN52	–10.06	–87.05	55.332	–77.502	Forest	Sporadic
NUN53	–11.96	–93.49	55.331	–77.502	Forest	Sporadic
NUN54	–11.07	–89.56	55.333	–77.503	Forest	Sporadic
NUN55	–11.86	–91.94	55.334	–77.502	Forest	Sporadic
NUN56	–11.84	–93.29	55.333	–77.502	Forest	Sporadic
NUN57	–9.30	–81.19	55.333	–77.500	Forest	Sporadic
NUN58	–10.82	–87.85	56.611	–76.215	Forest	Sporadic
NUN59	–12.26	–94.81	56.611	–76.216	Tundra	Discontinuous
NUN60	–13.30	–101.65	56.610	–76.215	Tundra	Discontinuous
NUN61	–12.94	–100.90	56.611	–76.214	Tundra	Discontinuous
NUN62	–13.36	–99.85	56.608	–76.217	Tundra	Discontinuous
NUN63	–11.39	–90.56	56.609	–76.217	Tundra	Discontinuous
NUN64	–11.11	–92.70	56.610	–76.214	Tundra	Discontinuous

Table A1 (*concluded*).

Lake	δ_L (^{18}O)	δ_L (^{2}H)	Latitude (° N)	Longitude (° W)	Vegetation	Permafrost
NUN65	–13.65	–104.51	56.610	–76.212	Tundra	Discontinuous
NUN66	–13.42	–104.72	56.609	–76.213	Tundra	Discontinuous
NUN67	–13.50	–104.09	56.610	–76.213	Tundra	Discontinuous
NUN68	–10.99	–92.09	56.609	–76.217	Tundra	Discontinuous
NUN69	–10.47	–90.24	56.609	–76.218	Tundra	Discontinuous
NUN70	–10.90	–88.95	56.608	–76.218	Tundra	Discontinuous
NUN71	–11.24	–91.90	56.608	–76.217	Tundra	Discontinuous
NUN72	–12.86	–100.82	56.608	–76.216	Tundra	Discontinuous
NUN73	–12.25	–95.42	56.609	–76.217	Tundra	Discontinuous
NUN74	–9.86	–84.74	56.611	–76.214	Tundra	Discontinuous
NUN75	–12.89	–93.14	56.924	–76.378	Tundra	Discontinuous
NUN76	–13.01	–93.81	56.924	–76.379	Tundra	Discontinuous
NUN77	–11.66	–90.62	56.923	–76.380	Tundra	Discontinuous
NUN78	–13.44	–100.80	56.923	–76.380	Tundra	Discontinuous
NUN79	–10.03	–83.45	56.924	–76.378	Tundra	Discontinuous
NUN80	–12.38	–94.39	56.923	–76.380	Tundra	Discontinuous
NUN81	–13.69	–100.87	56.924	–76.380	Tundra	Discontinuous
NUN82	–12.28	–94.46	56.924	–76.377	Tundra	Discontinuous
NUN83	–12.83	–93.40	56.924	–76.378	Tundra	Discontinuous
NUN84	–11.98	–89.36	56.923	–76.379	Tundra	Discontinuous
NUN85	–10.84	–87.35	56.924	–76.380	Tundra	Discontinuous
NUN86	–12.63	–94.84	56.924	–76.377	Tundra	Discontinuous

Note: ACP, Arctic Coastal Plain, Alaska; YF, Yukon Flats; OCF, Old Crow Flats; HBL, Hudson Bay Lowlands; NUN, Nunavik.